THE PENNSYLVANIA STATE UNIVERSITY

IONOSPHERIC RESEARCH

SCIENTIFIC REPORT ON

THE THEORY AND EXPERIMENTAL RESULTS OF AN IONOSPHERIC PROBE EXPERIMENT

by

Douglas S. Hoffman

January 10, 1966

SCIENTIFIC REPORT NO. 260

IONOSPHERE RESEARCH LABORATORY

The Pennsylvania State University
College of Engineering
Department of Electrical Engineering

NASA Grant NsG-134-61

Ionospheric Research

NASA Grant No. NsG-134-61

Scientific Report

on

"The Theory and Experimental Results of an Ionospheric Probe Experiment"

by

Douglas J. Hoffman

January 10, 1966

Scientific Report No. 260

"The research reported in this document has been sponsored by the National Aeronautics and Space Administration under Grant No. NsG-134-61."

Ionosphere Research Laboratory

Submitted by:

L. C. Hale

L. C. Hale, Assistant Professor
Electrical Engineering
Project Supervisor

J. S. Nisbet (acc)

J. S. Nisbet, Associate Professor
Electrical Engineering

Approved by:

A. H. Waynick

A. H. Waynick, Director
Ionosphere Research Laboratory

The Pennsylvania State University

College of Engineering

Department of Electrical Engineering

TABLE OF CONTENTS

ABSTRACT

13151

A multi-gridded probe experiment for the measurement of ionospheric parameters is described. A theoretical analysis of the operation of the probe under typical sounding rocket conditions indicates the performance to be expected in the determination of these parameters. In addition to the d.c. probe characteristics, the time derivative of the probe characteristics was also obtained in flight.

Data from the experiment which was flown on NASA Javelin 8.29 on May 19, 1965, at 4:11 p.m., local time, was analyzed in light of the theory. The following ionospheric parameters were obtained: an ion density profile for altitudes from 280 to 940 km, vehicle potential, and ion temperature.

The analysis showed that the probe ceased to function according to simple ram theory at the altitude where the ion sheath thickness was equal to the diameter of the probe assembly.

Some difficulties associated with ion probe measurements are pointed out, and practical suggestions for designing better ion probes are made.

Author

I. INTRODUCTION

1.1 Statement of the Problem

In order to obtain a direct measurement of ionospheric parameters, a retarding potential planar ion probe was flown on a rocket from Wallops Island, Virginia, on May 19, 1965, as part of the Mother-Daughter project which was a separating-payload propagation experiment for measuring electron densities. The payload was launched at 4:11 P. M., local time, on NASA Javelin 8.29, and the ion probe was mounted on the Mother section.

This analysis is concerned with the ion probe results from which it is theoretically possible to determine positive ion density, temperature, and composition, electron temperature, and vehicle potential in the ionosphere. The probe electronics was designed by L. C. Hale and its construction and operation is described in detail in his report, L. C. Hale (1964).

In addition to the direct current characteristics of the probe, the derivative of the current characteristics was also obtained experimentally in flight, and studies were made of the in-flight data processing circuitry to determine the optimum electronic circuit characteristics to obtain maximum information from the data. The derivative of the probe characteristics was investigated to determine if an evaluation of positive ion composition could be made.

The primary objective of this analysis was an accurate interpretation of the experimental data, taking into account any phenomena which may have affected the experimental results.

Modern engineering concepts have been applied to the processing of flight data both before and after transmission from the vehicle.

1.2 Review of Related Studies

An investigation of the ionosphere by means of direct probe measurements was made by the Russians, who used spherical ion probes on Sputnik III. Krassovsky (1959) indicated an electron temperature of not less than 15,000° K at an altitude of 795 km. Ion density measurements and large negative vehicle potentials were also reported.

The Russian results were questionable and Whipple (1959), through a theoretical development of the problem, was able to obtain a more plausible explanation of the Russian data. He derived the basic equations describing ion current to a retarding potential probe under the assumption of a Maxwellian velocity distribution of ions. Whipple's theoretical work is generally accepted, and in recent years, experimenters using planar probes have evaluated their data in light of his theoretical derivations.

Hanson (1962), using data from an ion probe experiment by Hale (1961), deduced the existence of helium ions above 1200 km. Hanson was able to construct a daytime model of the upper atmosphere, under high solar activity conditions, in which atomic oxygen ions predominate up to 1200 km altitude, helium ions from 1200 to 3400 km, and protons above 3400 km.

Bourdeau et al. (1962) used the Explorer VIII satellite to obtain direct ionospheric measurements. Values of positive ion concentration, electron temperature, and the ratio of atomic helium to oxygen ions were presented. The ratios of the ionic constituents

were determined by comparing experimental and theoretical probe characteristics. It was concluded that their model was consistent with an isothermal upper ionsophere in diffusive equilibrium.

The theory of measurement of positive ions by means of a two-electrode spherical probe was derived by Sagalyn and Smiddy (1963). They considered the case of a Maxwellian gas, where the vehicle velocity is variable with respect to the most probable ion velocity, and the mean free path is large compared to the probe dimensions. This theory was used to analyze experimental data and the results below the F_2 peak agreed to within 20 per cent with simultaneous ionosonde data.

Ion traps with plane geometry were flown on polar-orbiting satellites by Hanson, McKibbin, and Sharp (1964). One of their main objectives was to obtain a direct measurement of ion temperatures by measuring the ion velocity distribution. Earlier attempts had not been successful, yielding temperatures which were considered too high. The results of Hanson, McKibbin, and Sharp were not significantly improved. Computed ion temperatures were erratic and generally very high compared to neutral gas temperatures.

The data from the polar-orbiting satellites was not consistent with present day theories of the ionosphere because very low ion concentration and high satellite potentials were obtained for portions of the flight. It was pointed out that the satellite itself may have been capable of drastically modifying its immediate surroundings in some manner.

The results of nighttime measurements of positive ion

densities were presented by Sagalyn and Smiddy (1964). The ion scale height was found to change abruptly near 600 km and an ion temperature of $1050 \pm 50^{\circ}$ K was deduced from the ion scale height measured above the peak of the F region. In the region below the F peak, ion density values agreed to within 15 per cent with electron densities measured by local ionosonde stations. Vehicle potential varied only slightly from $-1.4 \pm .3$ volts for the altitude range from 300 to 1100 km. Above 700 km, the vertical ion profiles differed significantly from the results presented by other researchers in that large ion scale heights were obtained. The measured ion scale height was 2000 km at an altitude of 760 km.

A significant result of Sagalyn and Smiddy's analysis was a determination of the ionic constituents without making assumptions about a reference level composition. Using a general expression for N(z), the ion density, in terms of altitude, ion mass, and temperature, the relative proportions of the ionic constituents at a reference level were determined by comparing experimental profiles with general solutions of N(z) for a range of reference level compositions and temperatures.

1.3 Description of the Instrument

A retarding potential planar probe was used to make direct ionospheric measurements. The grid structure and associated voltage waveforms are shown in Figure 1. Four tungsten grids of 1 mil wire were welded to tungsten rings which were supported by 3 mm thick Teflon spacers. The tungsten collector plate was 1-5/8" in diameter and the aperture was 1" in diameter.

The probe operated alternately in ion and electron modes

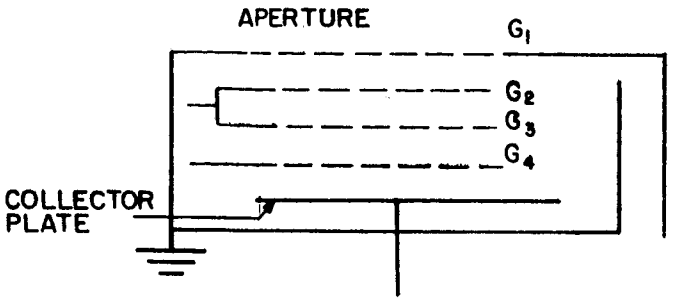

PROBE ASSEMBLY

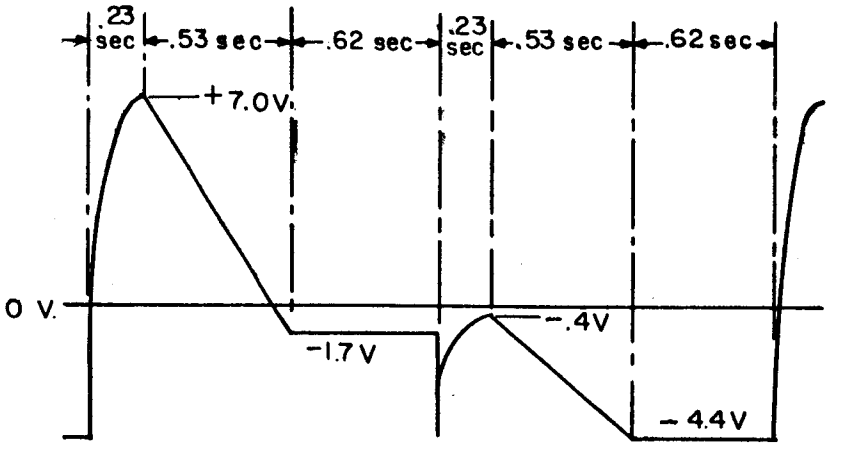

SWEEP WAVEFORM ON GRIDS 2&3

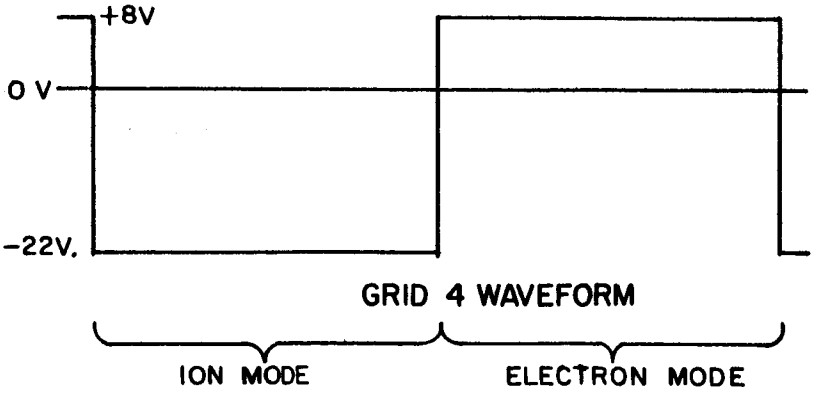

PROBE ASSEMBLY AND VOLTAGE WAVEFORMS

FIGURE 1

with grid G_1 tied to vehicle ground at all times. A linear sweep voltage was applied to grids G_2 and G_3 which were connected together to establish a more uniform potential barrier. In the ion mode a negative voltage on grid G_4 suppressed environmental electrons and photo electrons from the collector plate. The collector plate was held at vehicle potential by a high-gain feedback electrometer circuit which served as a current measuring device.

An RC differentiator and a gain of 50 d. c. amplifier were used to obtain the derivative of the output of the electrometer circuit. The derivative information was fed directly to telemetry.

An automatic range switching circuit was employed to extend and improve the current measuring sensitivity of the instrument which was used with a standard 0 to 5 volts telemetry channel.

II. THEORETICAL DEVELOPMENT OF THE PROBLEM

2.1 Probe Characteristics

The expression for ion current to a retarding potential planar probe has been derived. These derivations are not original but are presented because of their major importance to this analysis. Whipple (1959) and others have discussed these derivations and their implications.

A fixed co-ordinate system is chosen with positive x axis in the direction of the vehicle velocity, and an ion with a thermal velocity component c in this direction has a relative velocity component $v_r = c-V$ with respect to the vehicle, where V is the vehicle velocity. A Maxwellian velocity distribution is assumed and is given by

$$\frac{dN}{dc} = \frac{Ne^{-(c/a)^2}}{a\sqrt{\pi}} \quad , \tag{2.1}$$

where N is the ambient ion density, and a is the most probable ion velocity defined by

$$a = \sqrt{2kT/m} \quad ,$$

where k = Boltzman's constant

T = ion temperature in degrees Kelvin

m = ion mass .

The collector current is

$$I = \int \alpha e A v_r \, dN \quad , \tag{2.2}$$

where A is the collector area, α is a grid transparency coefficient, and e is the ionic charge. Only those ions with a kinetic energy toward the rocket greater than the retarding potential barrier are collected, that is for

$$\frac{1}{2} m v_r^2 > e\phi \quad .$$

The ions with sufficiently large negative velocities are collected and the collector current is

$$I = \frac{\alpha e A N}{a\sqrt{\pi}} \int_{-\infty}^{-\sqrt{2e\phi/m}} v_r e^{-(v_r+V)^2/a^2} dv_r \quad . \qquad (2.3)$$

After integrating,

$$I = \alpha e A N V \left(\frac{1}{2} + \frac{1}{2} \operatorname{erf}(x) + \frac{a e^{-x^2}}{2V\sqrt{\pi}}\right) \quad , \qquad (2.4)$$

where $$x = \frac{1}{a} \left(V - \sqrt{2e\phi/m}\right) \qquad (2.5)$$

and $$\operatorname{erf}(x) = \frac{2}{\sqrt{\pi}} \int_0^x e^{-y^2} dy \quad . \qquad (2.6)$$

Equation 2.4 is the well known equation for ion current to a retarding potential probe when the thermal velocity of ions is small compared to the vehicle velocity. V is the effective component of rocket velocity along the axis of the probe so that there would be a factor of cos θ in these derivations where θ is the angle between the rocket velocity vector and the normal to the planar probe.

A computer program was written to tabulate ion probe

current as a function of the sweep voltage with vehicle velocity, ion temperature, ion density, and plasma composition as parameters. The results were curves of collector current versus sweep voltage for the various parameters.

The Javelin rocket on which this experiment was flown reaches a peak altitude of approximately 1000 km so that a binary mixture of He^+ and O^+ was assumed since these will be the dominant ions at these altitudes (Hanson, 1962). Equation 2.7 was used to determine probe current since, when more than one ion species is present, the total current is the sum of the individual currents.

$$I = \alpha e A N_1 V \left(\frac{1}{2} + \frac{1}{2} \operatorname{erf}(x_1) + \frac{a_1 e^{-x_1^2}}{2V\sqrt{\pi}} \right) + \alpha e A N_2 V \left(\frac{1}{2} + \frac{1}{2} \operatorname{erf}(x_2) + \frac{a_2 e^{-x_2^2}}{2V\sqrt{\pi}} \right) \qquad (2.7)$$

The subscripts 1 and 2 refer to values for oxygen and helium.

There are no thermal components of ion velocity at a temperature of 0° and then the current curves should have sharp well-defined steps. This special case was checked for a temperature of 1° K and the results are shown in Figure 2. The steps should occur at voltages where the kinetic interaction energy, due to the rocket velocity, is equal to the potential barrier.

$$\frac{1}{2} m V^2 = e\phi \qquad (2.8)$$

For O^+ and He^+, ϕ was calculated to be .70 and .175 volts for a vehicle velocity of 2.9 km/sec. The results, as tabulated from the

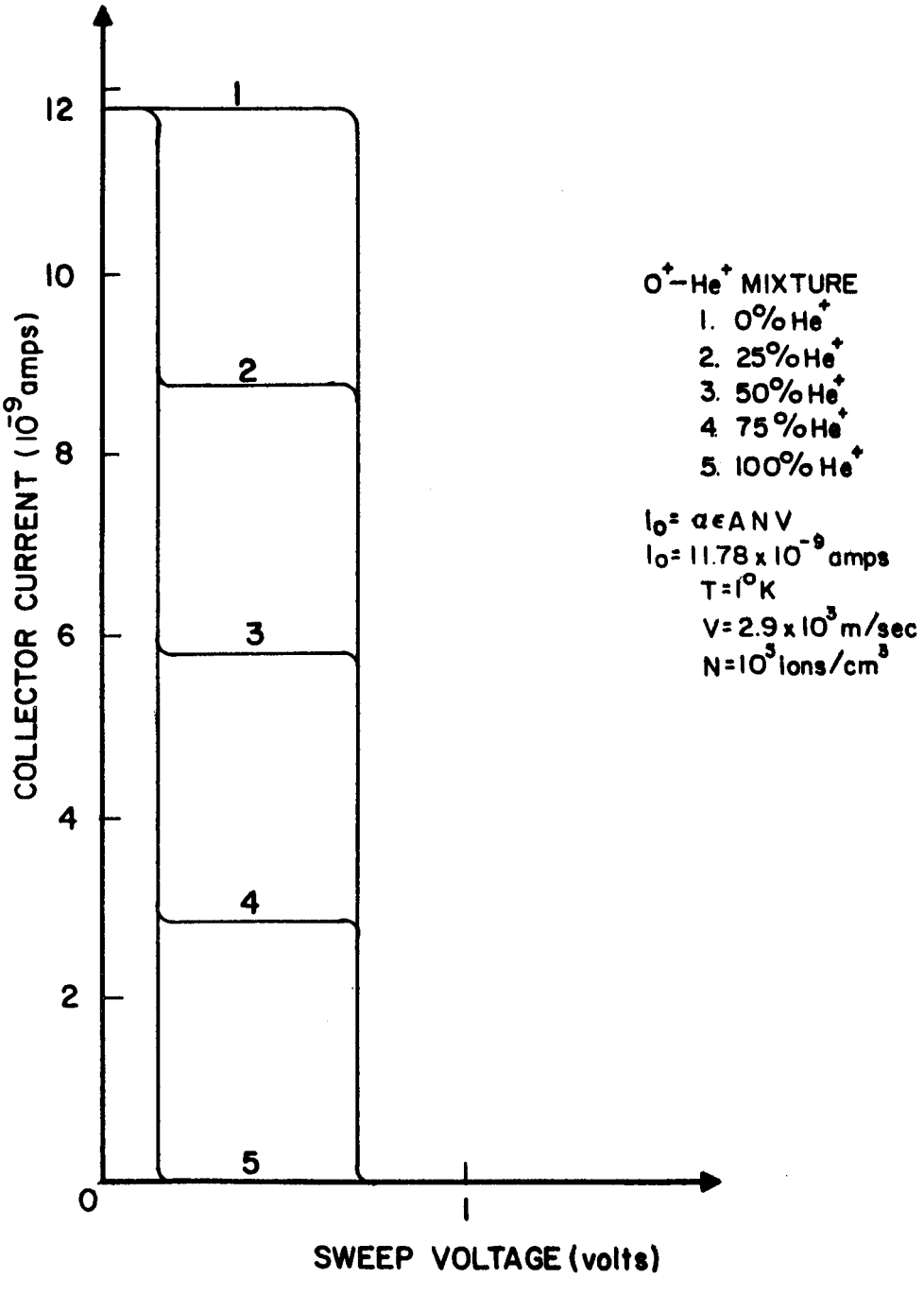

PROBE CURRENT WITH NO THERMAL COMPONENTS OF ION VELOCITY

FIGURE 2

computer program and illustrated in Figure 2, agree with these calculations.

Figure 3 illustrates calculated current curves from equation 2.7 and corresponds to these conditions:

$V = 2.9$ km/sec

$T = 1200^{\circ}$ K

$N = 10^5$ ion/cm^3

$A = 5.07$ cm^2

$\alpha = 0.5$

It is seen that the effect of the thermal velocities is to smooth out the curves. Thus, an accurate determination of plasma composition cannot be made from these curves since they vary only slightly from each other, even though the composition varies by 25 per cent He^+ steps.

R. E. Bourdeau et al. (1962) have fitted experimental data to theoretical curves of the type shown in Figure 3, and from the best fit they determined the ratio of the ionic constituents. Typical results for He^+/O^+ at an altitude of 1630 km were $1.3 \pm .3$ which corresponds to an error of $\pm 23\%$. They state that this error estimate is optimistic in view of the assumptions made (θ was assumed to be constant even though it varied by 25° during the period required to obtain one current curve).

One objective of this analysis is to determine if it is possible to obtain more accurate data on ion composition utilizing information from the derivative of the probe characteristics.

2.2 Derivative of Probe Characteristics

The derivative of collector current with respect to sweep voltage is

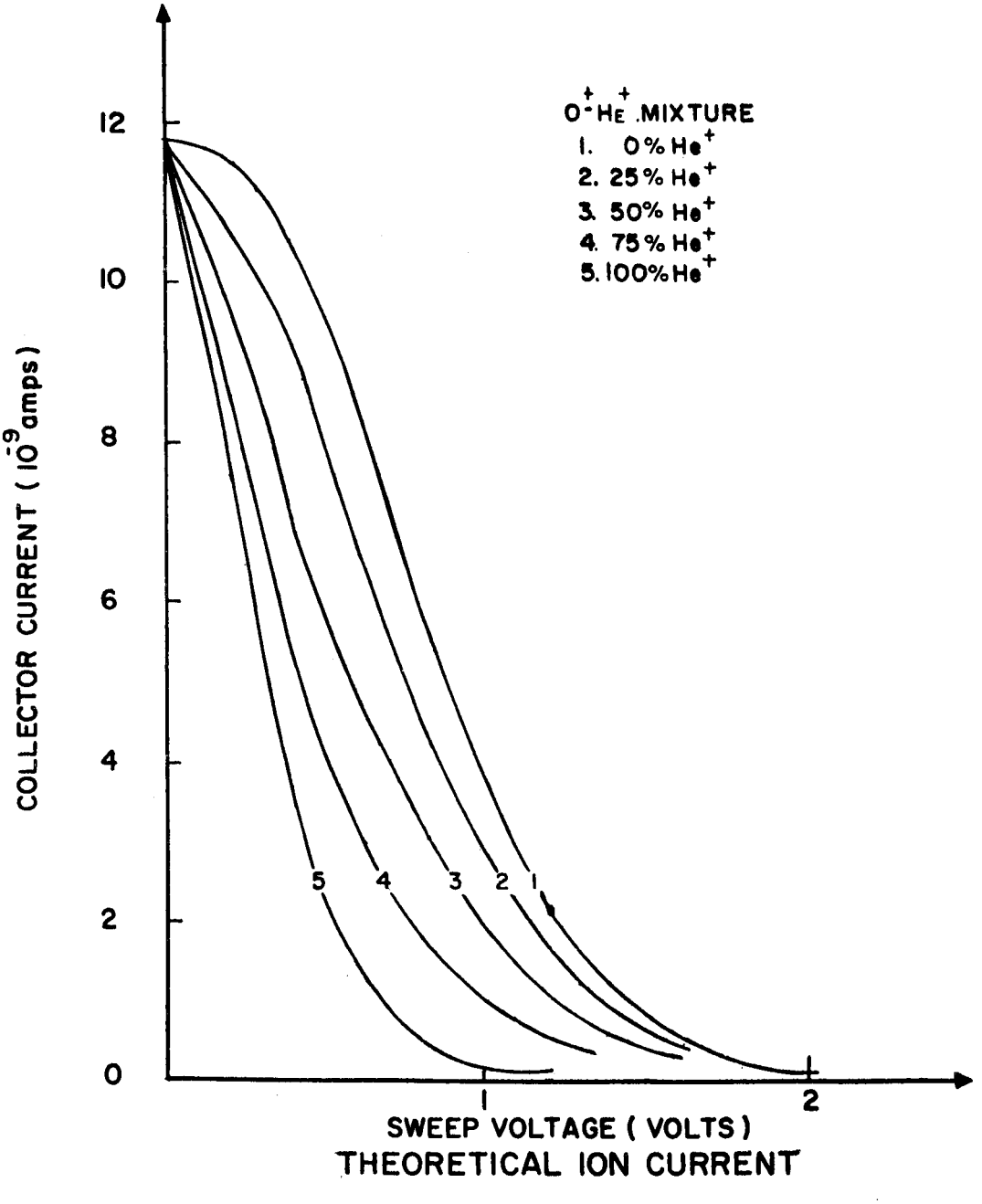
O^+-He^+ MIXTURE
1. 0% He^+
2. 25% He^+
3. 50% He^+
4. 75% He^+
5. 100% He^+
COLLECTOR CURRENT (10^{-9} amps)
12
10
8
6
4
2
0
1
2
5
4
3
2
1
SWEEP VOLTAGE (VOLTS)
THEORETICAL ION CURRENT

FIGURE 3

$$\frac{dI}{d\phi} = \alpha eANV\left(\frac{1}{2}\ \frac{d}{d\phi}\ \mathrm{erf}(x) + \frac{ae^{-x^2}}{2V\sqrt{\pi}}(-2x)\ \frac{dx}{d\phi}\right) \quad , \qquad (2.9)$$

where $$\frac{dx}{d\phi} = \frac{-1}{a}\ \sqrt{e/2m\phi} \qquad (2.10)$$

and $$\frac{d}{d\phi}\ \mathrm{erf}(x) = \frac{-1}{a}\ \sqrt{2e/\pi m\phi}\ \ e^{-x^2} \quad . \qquad (2.11)$$

After substituting equations 2.10 and 2.11 into equation 2.9,

$$\frac{dI}{d\phi} = \alpha eANV\sqrt{e/2\pi m\phi}\ \left(\frac{xe^{-x^2}}{V} - \frac{e^{-x^2}}{a}\right) \quad . \qquad (2.12)$$

Equation 2.12 for the derivative of current with respect to sweep voltage was plotted with the results shown in Figure 4. These curves were obtained using the same parameters as were used to obtain the current curves of Figure 3. The vertical axis corresponds to negative values of $\frac{dI}{d\phi}$. This is as expected, since, as the retarding sweep voltage increases, positive ion current decreases causing $\frac{dI}{d\phi}$ to be negative. As the per cent He^+ increases, the location of the peak shifts to the left and the peak amplitude first decreases and then increases as the per cent He^+ increases.

A possible method for determining ionic composition would be to fit experimental results to these theoretical models. It is obvious that because the curves vary more significantly from each other, this would be more accurate than the previously described method of comparing the current curves. However, these are ideal curves and are not the exact results that are obtained after passing the signal through electronic circuitry.

2.3 Analysis of Differentiating Circuit

The differentiating circuitry is shown in Figure 5. The

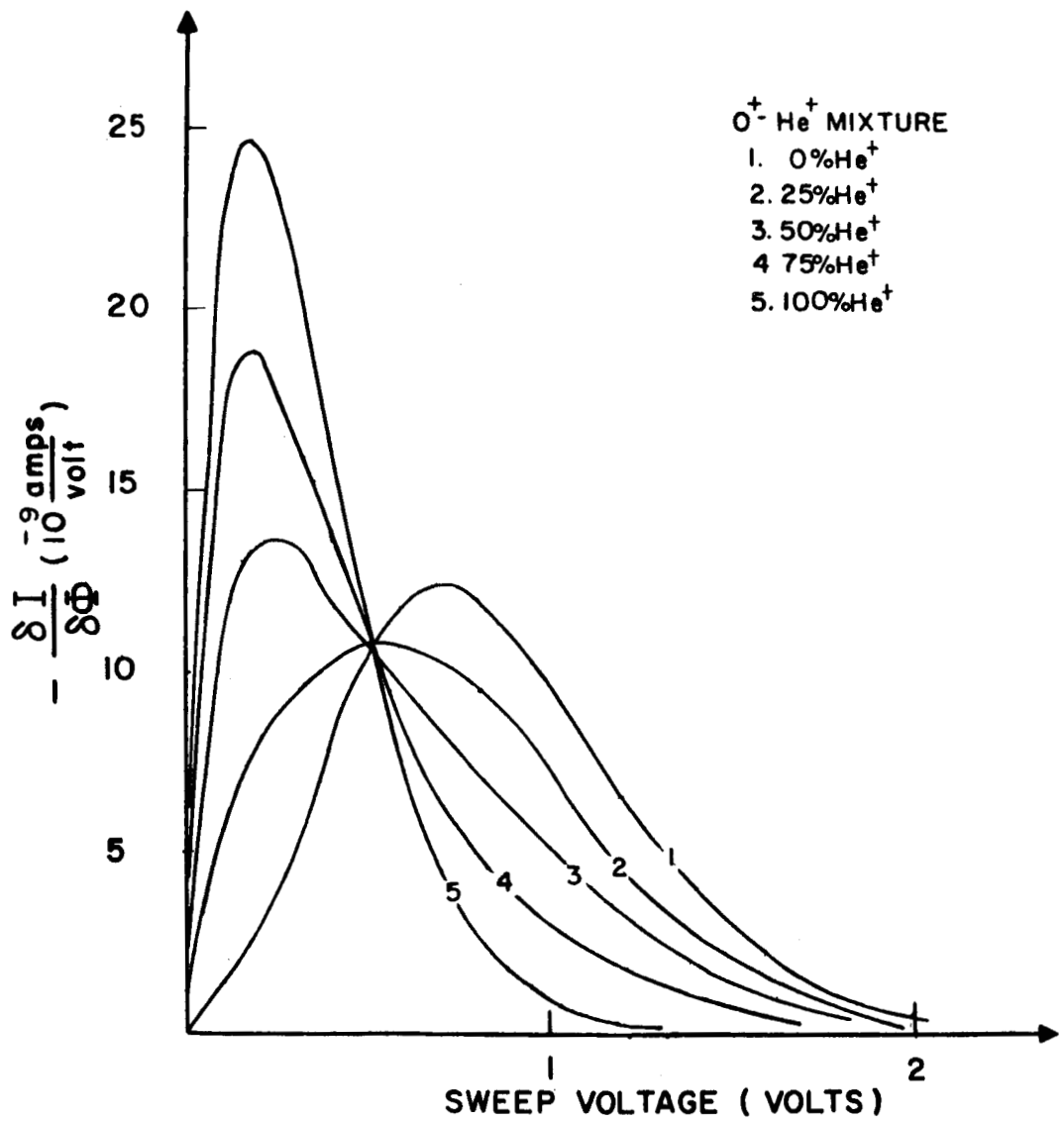

DERIVATIVE OF PROBE CHARACTERISTICS

FIGURE 4

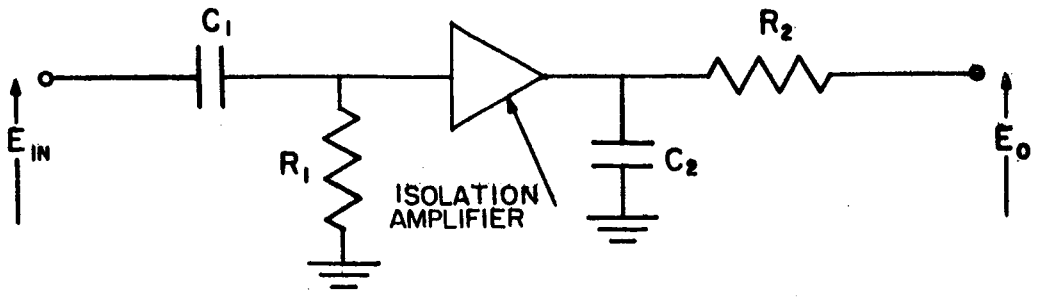

DIFFERENTIATING AND OUTPUT CIRCUIT

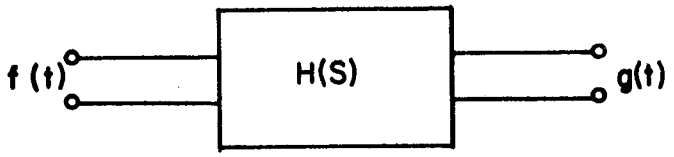

LINEAR TWO-PORT NETWORK
TRANSFER FUNCTION $H(S) = G(S)/F(S)$

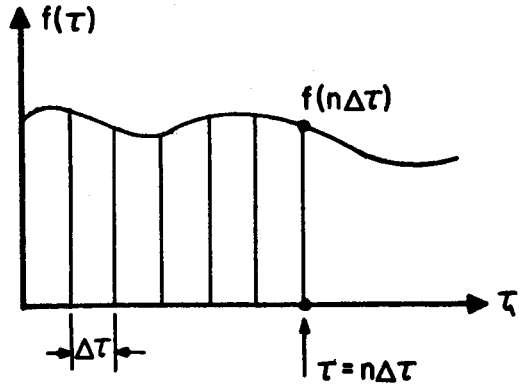

IMPULSE REPRESENTATION OF FUNCTION

DIFFERENTIATING CIRCUIT AND INPUT APPROXIMATION

FIGURE 5

combination of R_1 and C_1 serve as a differentiator while R_2 and C_2 filter the output. The amplifier is considered to be an ideal isolation amplifier with infinite input and zero output impedance and a gain of one. This d.c. amplifier actually has a gain of 50 but the gain has been taken as one in the following calculations.

The derivative is obtained experimentally with the circuit of Figure 5, and it is useful to study the output as a function of the RC time constants. A straightforward mathematical circuit analysis is not possible because of the complexity of the input ion current function. It was decided that an impulse technique would be used since the response of networks to other input functions can be determined from the impulse response. See M. Schwartz (1959) for a discussion of the following method of analysis.

The network was analyzed utilizing the convolution integral which is given by

$$g(t) = \int_{-\infty}^{\infty} f(\tau)\, h(t-\tau)\ d\tau \quad . \tag{2.13}$$

As shown in Figure 5, g(t) is the output function, f(t) is the input, and h(t) is the network transfer function in the time domain and is found as the time response if an impulse is applied to the network. The network response may be considered a weighted sum of different values of f(t) with h(t) as the weighting function. The integral definition of an impulse is approximated by a sum so that f(t) is represented by a series of impulses of varying weight.

$$f(t) = \int_{-\infty}^{\infty} f(\tau)\ \ \delta(t-\tau)\ d\tau \tag{2.14}$$

$$f(t) \simeq \sum_{n=-\infty}^{\infty} f(n\Delta\tau)\ \delta(t-n\Delta\tau)\ \Delta\tau \qquad (2.15)$$

If f(t) is applied to a linear system, the response can be found by superimposing the response of each of the impulses of equation 2.15. The response of an impulse $A\ \delta(t-n\Delta\tau)$ is by definition $Ah(t-n\Delta\tau)$, so that the output is given by

$$g(t) \simeq \sum_{n=-\infty}^{\infty} f(n\Delta\tau)\ h(t-n\Delta\tau)\ \Delta\tau \quad . \qquad (2.16)$$

In the limit as $\Delta\tau$ approaches 0, $n\Delta\tau$ approaches τ and the sum becomes the convolution integral, equation 2.13.

For the circuit of Figure 5, the transfer function is

$$H(s) = \frac{s\tau_1}{(s\tau_1 + 1)\ (s\tau_2 + 1)} \quad . \qquad (2.17)$$

This corresponds to an impulse response, time function

$$h(t) = -\frac{c}{\tau_1\tau_2}\ e^{-t/\tau_1} + \frac{c}{\tau_2^2}\ e^{-t/\tau_2} \quad , \qquad (2.18)$$

where $c = (1/\tau_2 - 1/\tau_1)^{-1}$.

From equation 2.16 and 2.18, we find that

$$g(t) \simeq \sum_{n=-\infty}^{\infty} f(n\Delta\tau)\ \left(-\frac{c}{\tau_1\tau_2}\ e^{-(t-n\Delta\tau)/\tau_1} + \frac{c}{\tau_2^2}\ e^{-(t-n\Delta\tau)/\tau_2}\right)\Delta\tau \quad . \qquad (2.19)$$

Equation 2.19 can be applied to find the output for an arbitrary input f(t) which for this case will be the waveforms shown in Figure 3.

Experimentally, a high gain d.c. operational amplifier with a feedback resistance R_F is used to convert the input current to a voltage level. Ideally,

$$E = - I_{IN} R_F \quad . \tag{2.20}$$

$R_F = 10^8$ ohms so that an input of 10^{-9} amps corresponds to a voltage input of -0.1 volts to the differentiator.

A computer program was written to solve equation 2.19 with the results being plots of output voltage versus sweep voltage. The upper limit of the summation was set by the fact that $h(t-\tau) = 0$ for τ larger than t which means that future inputs do not affect the present response. Any term more than six time constants in the past can be neglected since its response has essentially decayed to zero and thus the lower limit was found. The sampling interval, $\Delta\tau$, was taken as 0.1 of the smallest τ because the exponential can vary only slightly in that interval of time.

In the first set of curves, Figures 6 through 9, τ_2 is constant and τ_1 varies. It is clear that these curves are not as distinctive as the ideal derivatives of Figure 4. The waveforms have been attenuated and the duration of the response is longer, but they do have the same general shape as the ideal derivatives.

Figures 6 and 7, for τ_1 = .1 sec and .059 sec, are very similar so that the effect of decreasing τ_1 is negligible. As the

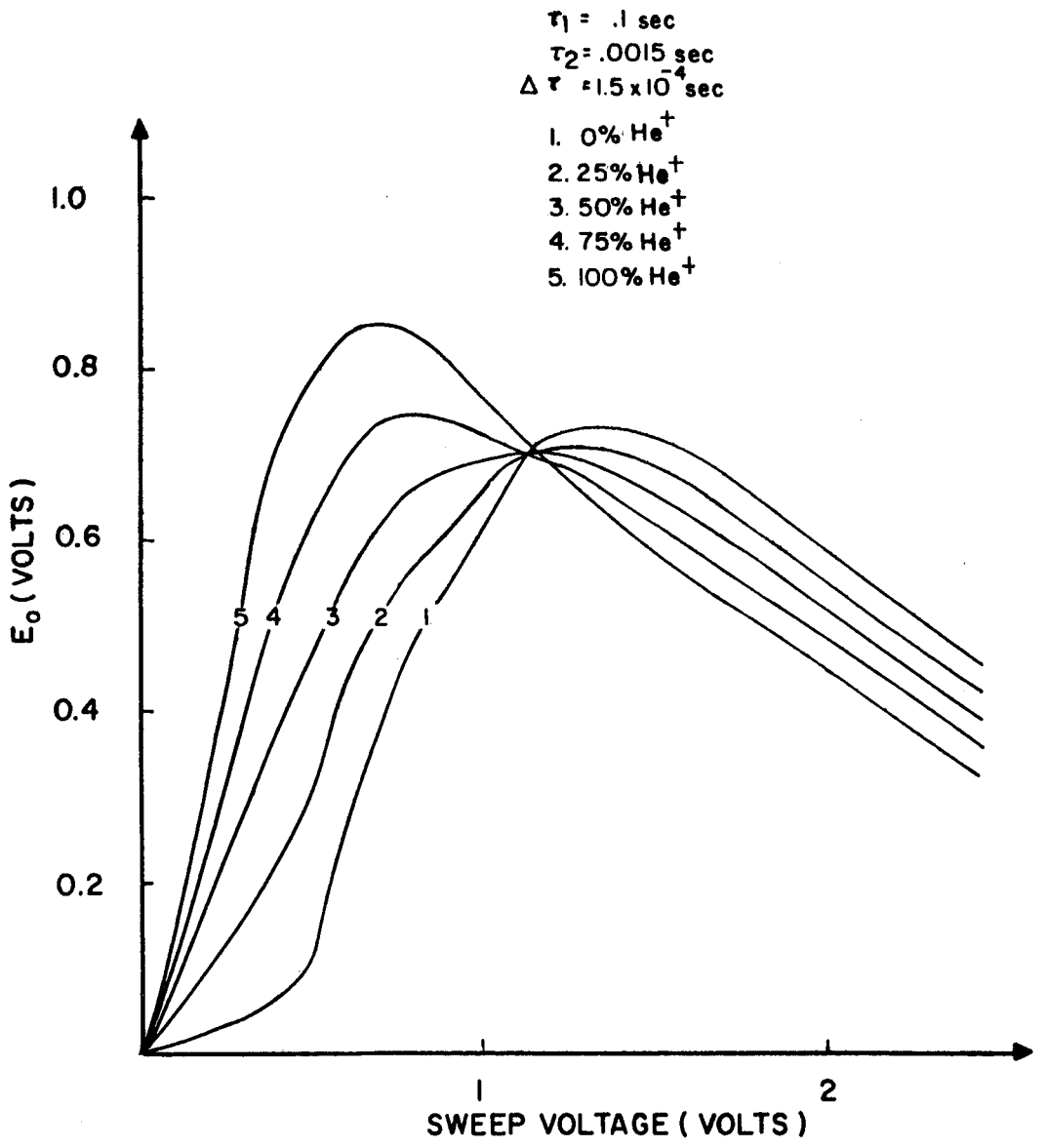

DIFFERENTIATOR OUTPUT USING IMPULSE TECHNIQUE

FIGURE 6

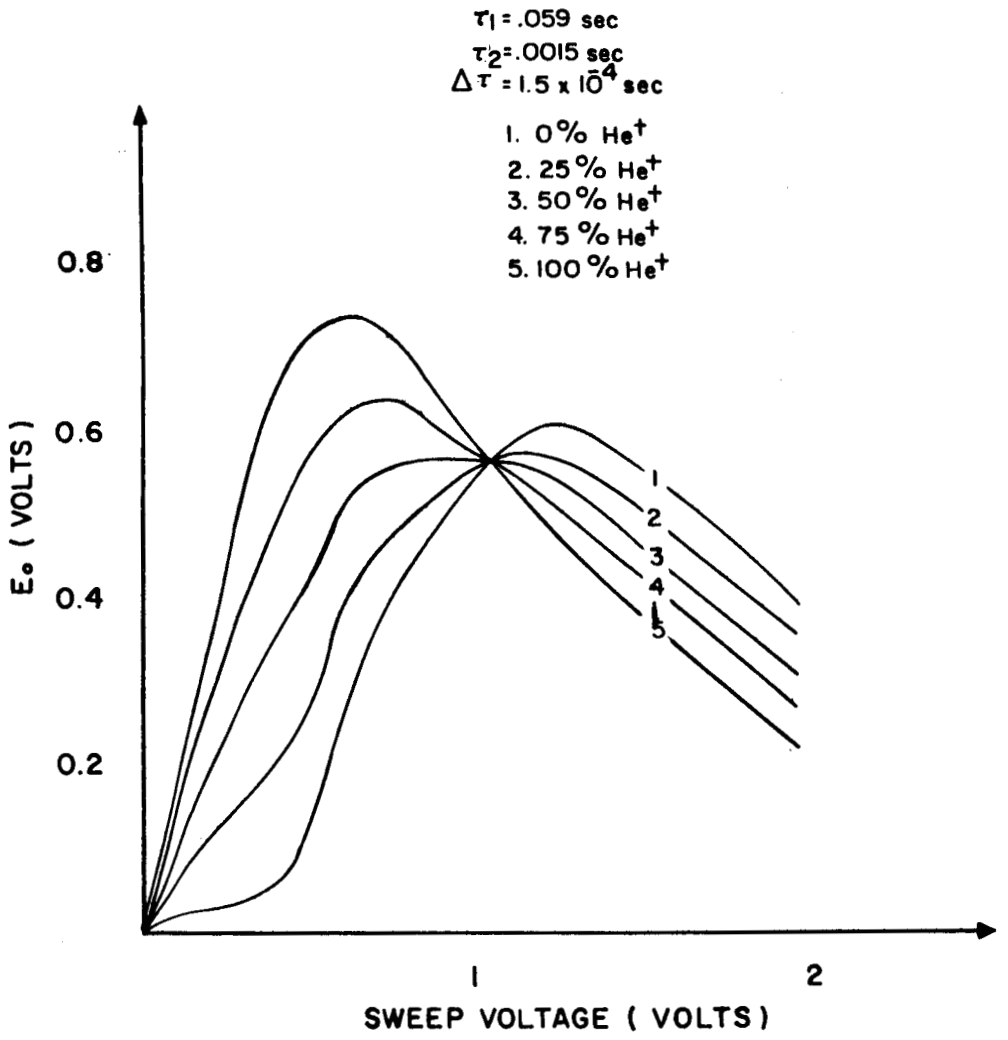

DIFFERENTIATOR OUTPUT USING IMPULSE TECHNIQUE

FIGURE 7

per cent He^+ is increasing in the region from 0% to about 75% of the total composition, the peak amplitude varies only slightly, and the position of the peak shifts to the left. These curves offer little in the way of a improved method for determining plasma composition. In the region from 75% to 100% He^+, it might be possible to determine plasma composition from the peak amplitude, but for lower percentages it would be difficult to apply this method of analysis.

In Figure 8, it is seen that for $\tau_1 = .02$ sec, the amplitude has decreased to approximately half the levels of Figure 6, and the network response has been damped out more quickly.

Figure 9 offers some possibilities for determining the ionic constituents. Amplitude measurements near a sweep voltage of 0.4 volts would be useful. Curve fitting of experimental results to theoretical models could also be employed, since the shape of different per cent He^+ plots vary appreciably from each other. A double peak can be seen on the number 3 curve, and corresponds to the time response of the network being fast enough so that it is possible to distinguish between the He^+ and O^+ being retarded.

Figure 10 is a comparison of the waveforms for different values of τ_1, with a 50% He^+ mixture. Curves 1, 2, and 3 are almost identical except that the signal level is decreasing as τ_1 decreases. The time response is such that the effects of He^+ and O^+ are distinguishable in curve 4 (the first peak being the response to He^+ and the second being due to O^+).

In Figure 11, the time constant of the output circuit was changed, and it was noted that no new information was obtained by observing the output as a function of τ_2.

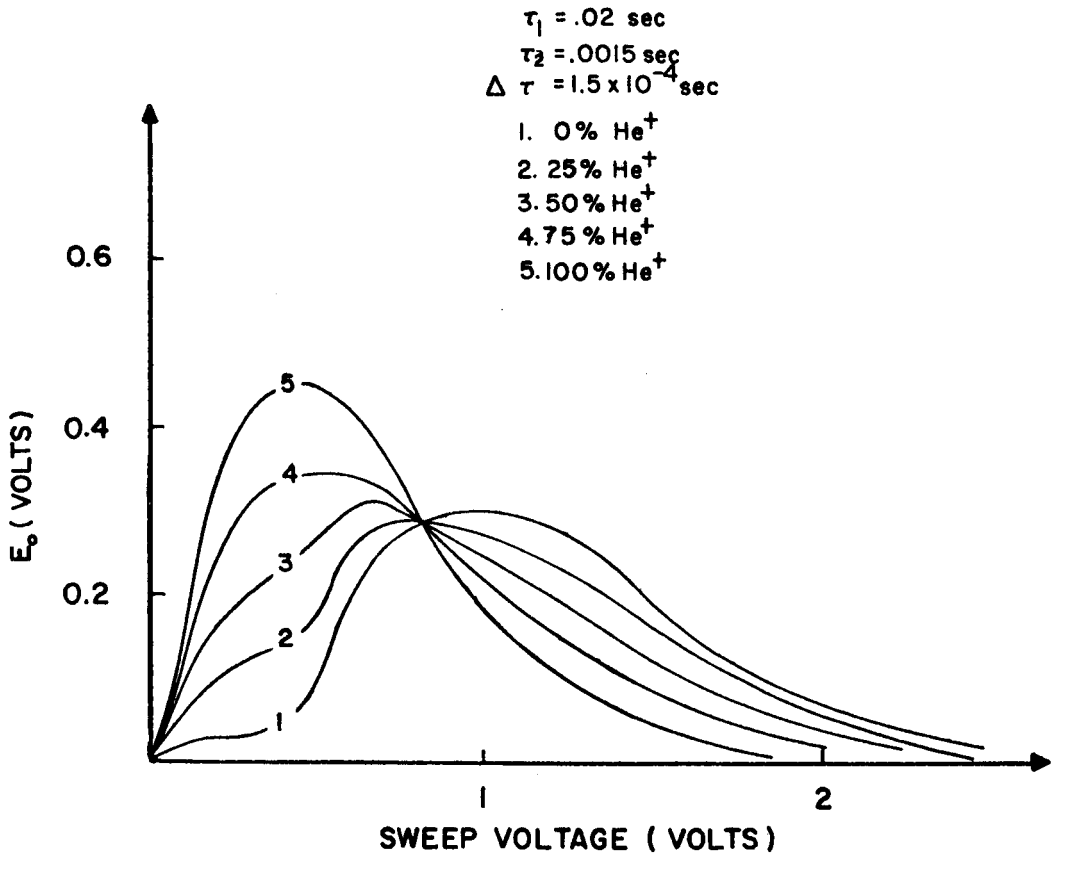

DIFFERENTIATOR OUTPUT USING IMPULSE TECHNIQUE

FIGURE 8

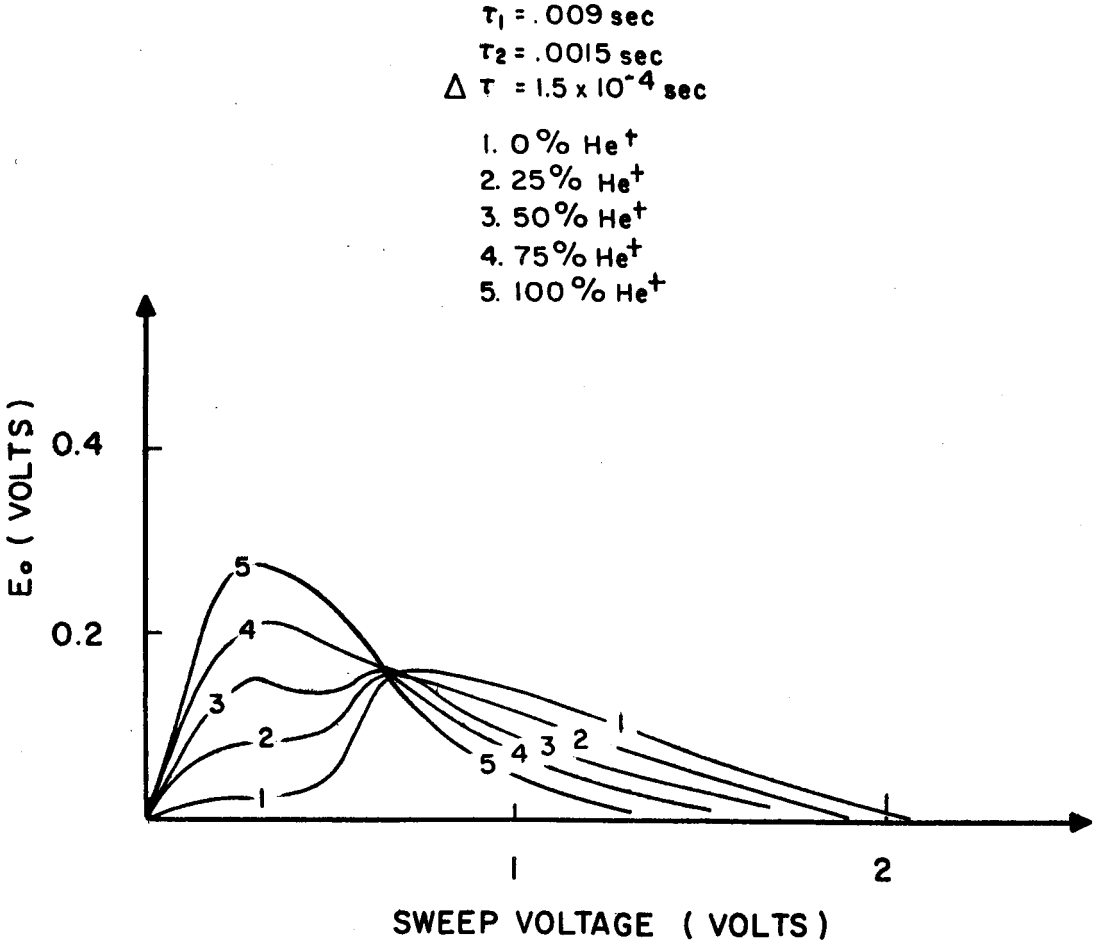

DIFFERENTIATOR OUTPUT USING IMPULSE TECHNIQUE

FIGURE 9

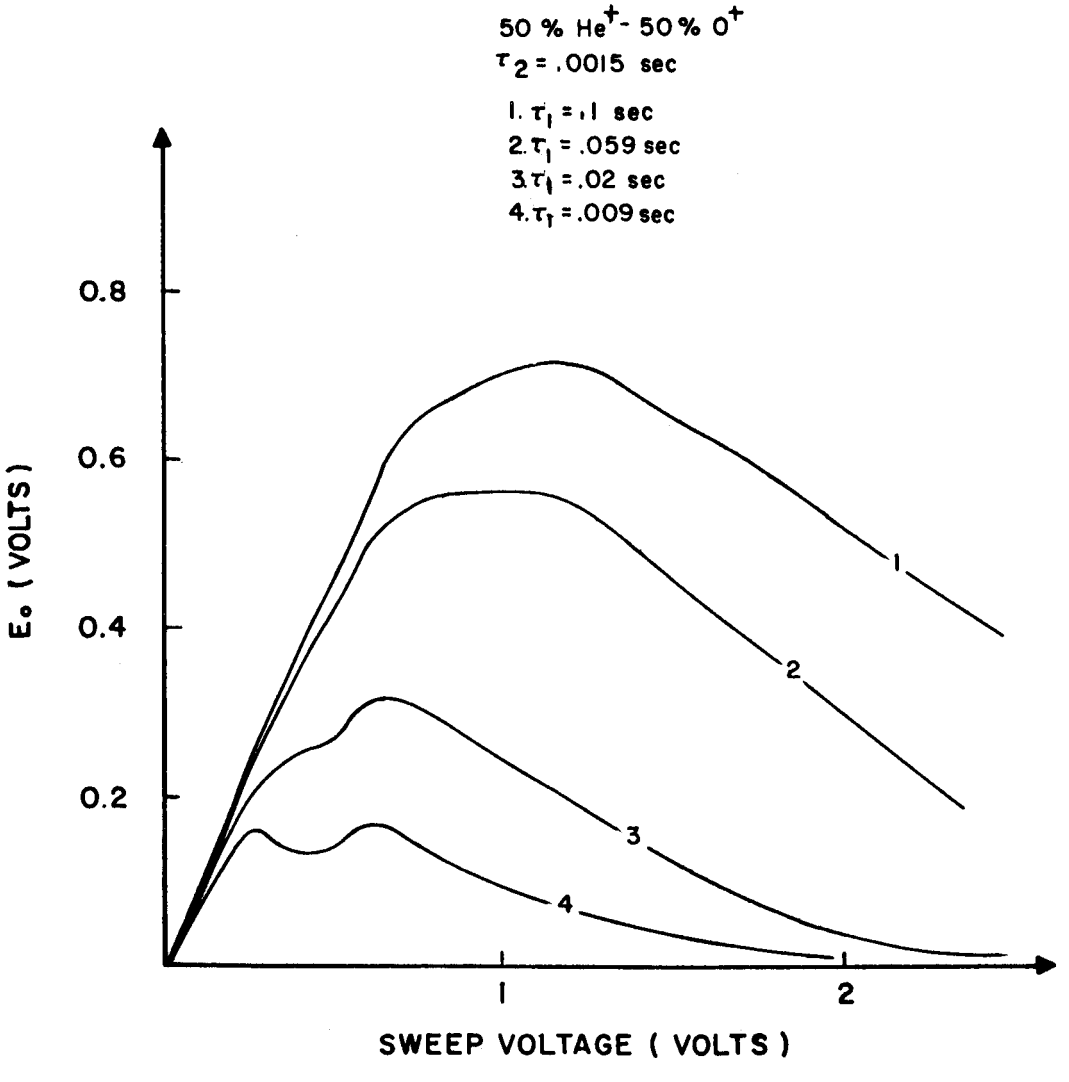

DERIVATIVE WAVEFORMS FOR VARIOUS VALUES OF τ_1

FIGURE 10

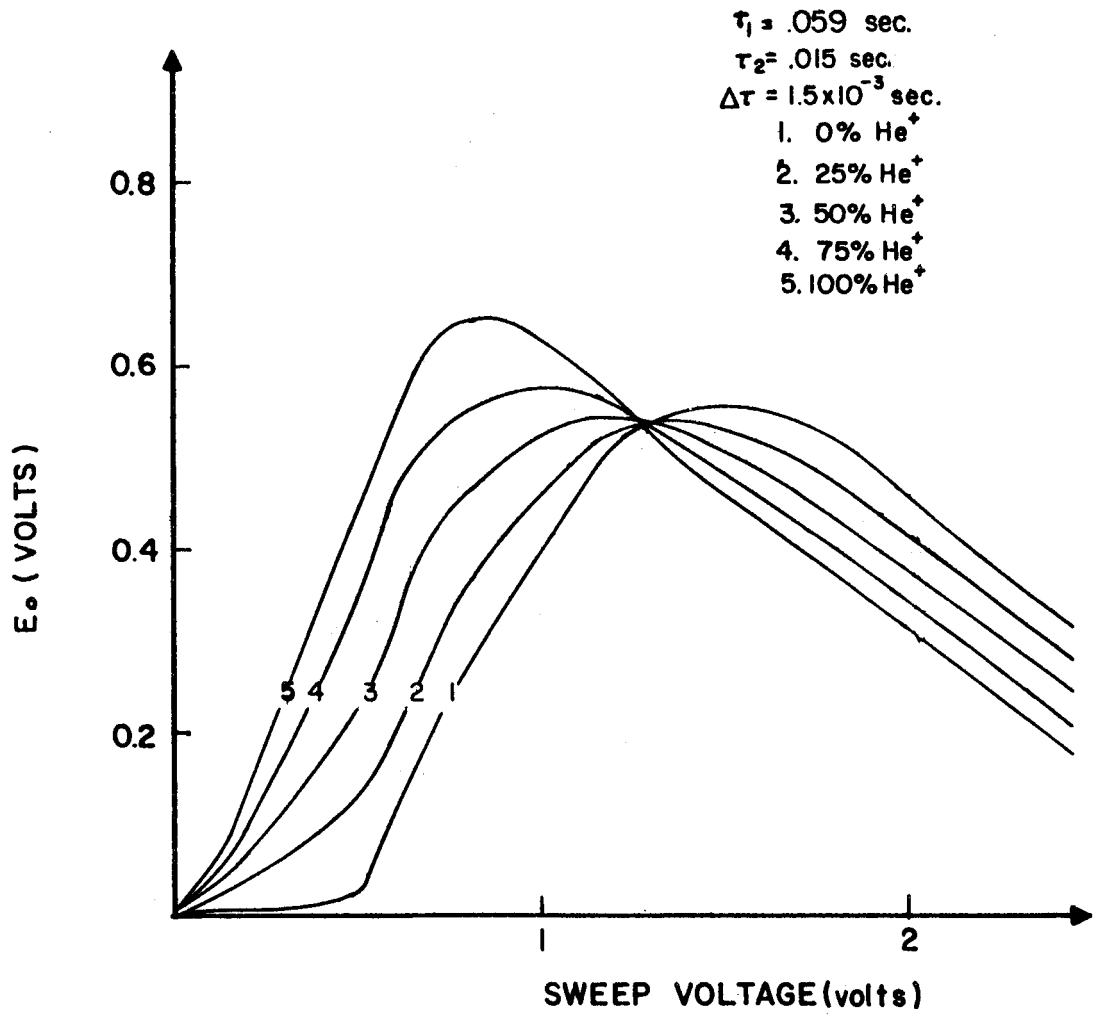

DIFFERENTIATOR OUTPUT USING IMPULSE TECHNIQUE

FIGURE 11

The general shape of the derivative characteristics, Figures 6 through 11, is correct. A sufficient number of terms were included in the series approximation (equation 2.19) so that any error is reasonably small.

III. EXPERIMENTAL RESULTS

3.1 Ion Density

When the total potential goes negative so that nearly all ions in the path of the aperture are collected, equation 2.7 reduces to a simple form, provided the vehicle velocity is much greater than the most probable ion velocity. Positive ion current is then approximated by equation 3.1, where the angle θ is shown explicitly.

$$I = \alpha eANV \cos\theta \qquad (3.1)$$

From this equation, ion density was determined at saturation since all other parameters were known.

For the probe used on the Mother-Daughter payload, the transmission coefficient of a single grid was found to be .93 by determining the fraction of the grid area, which was unobstructed by the wires. A total coefficient of .74 was obtained by raising .93 to the fourth power since four grids were used.

The instrument calibration curve is shown in Figure 12; the input calibration voltage was applied through a 10^9 ohm resistor with the other side being held at ground potential on the collector plate of the probe. Thus, a calibration input of 1 volt corresponds to an ion current of 10^{-9} amps to the collector plate. The range switching features are evident in Figure 12 and give the probe greater flexibility.

The necessary trajectory information for determining the ion density profile is shown in Figures 13, 14, and 15. Figure 13 is a plot of altitude versus flight time, while Figure 14 is a plot of vehicle velocity versus flight time. Figure 15 illustrates how the

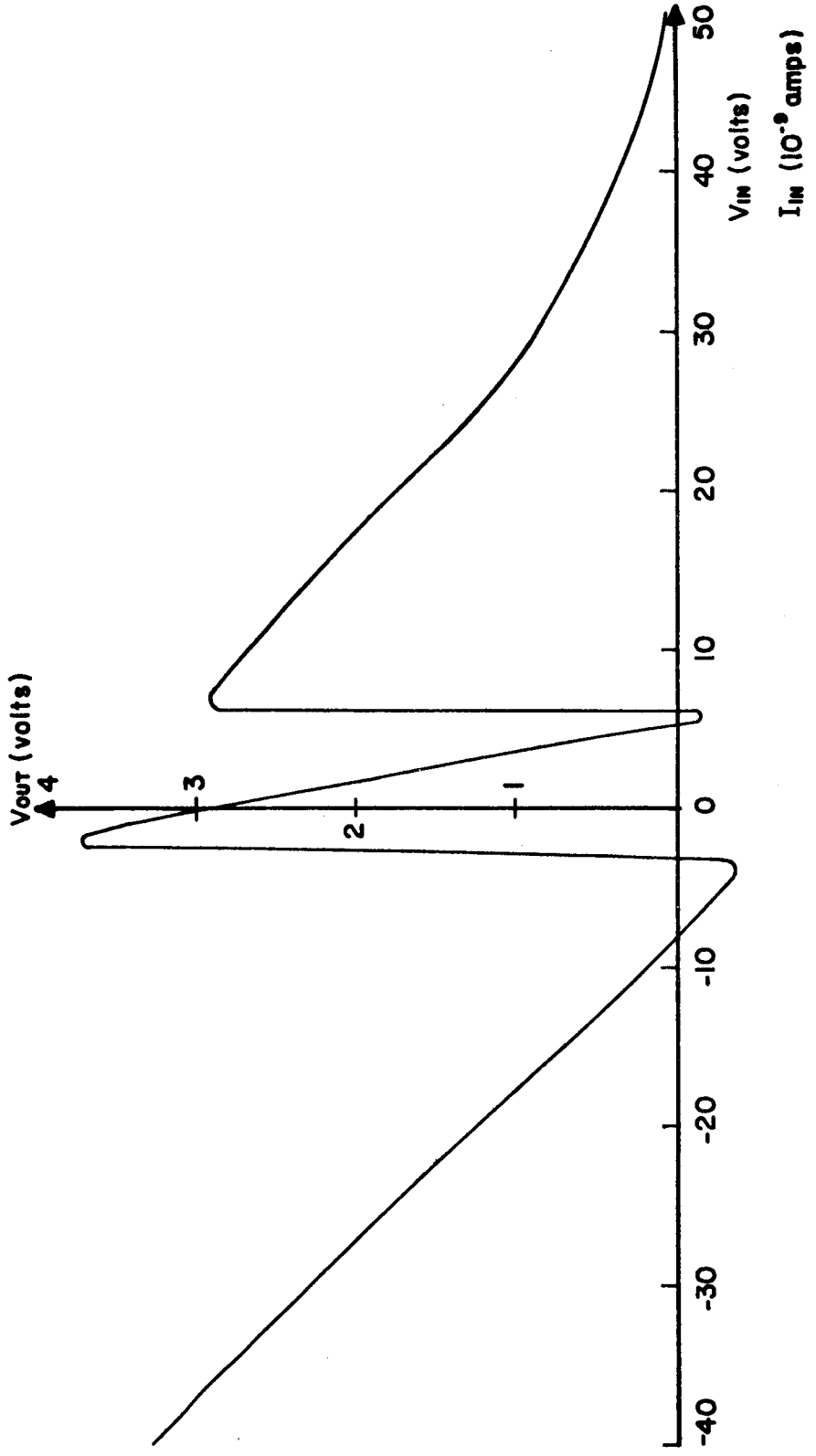

PROBE CALIBRATION CURVE

FIGURE 12

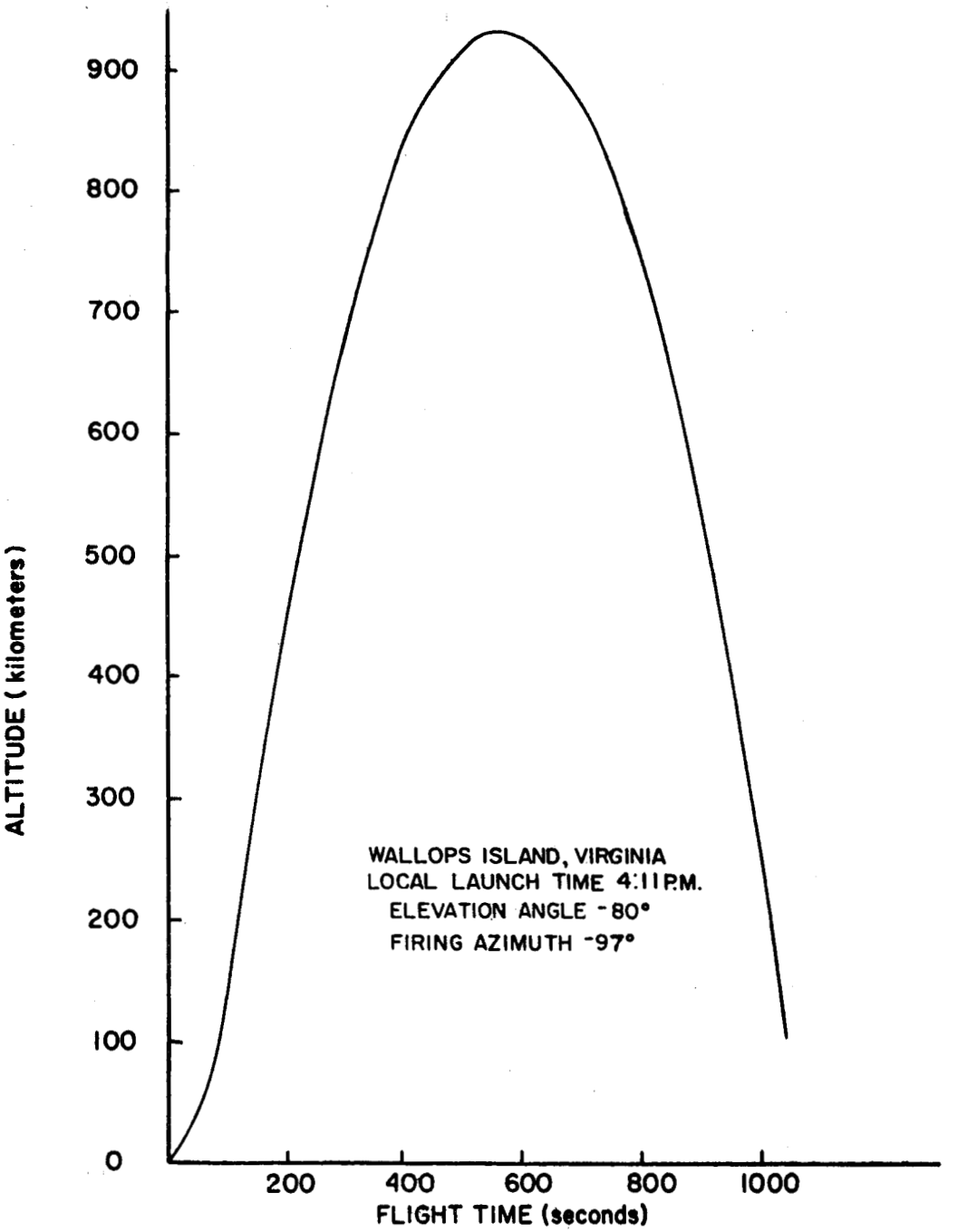

TRAJECTORY NASA JAVELIN 8.29

FIGURE 13

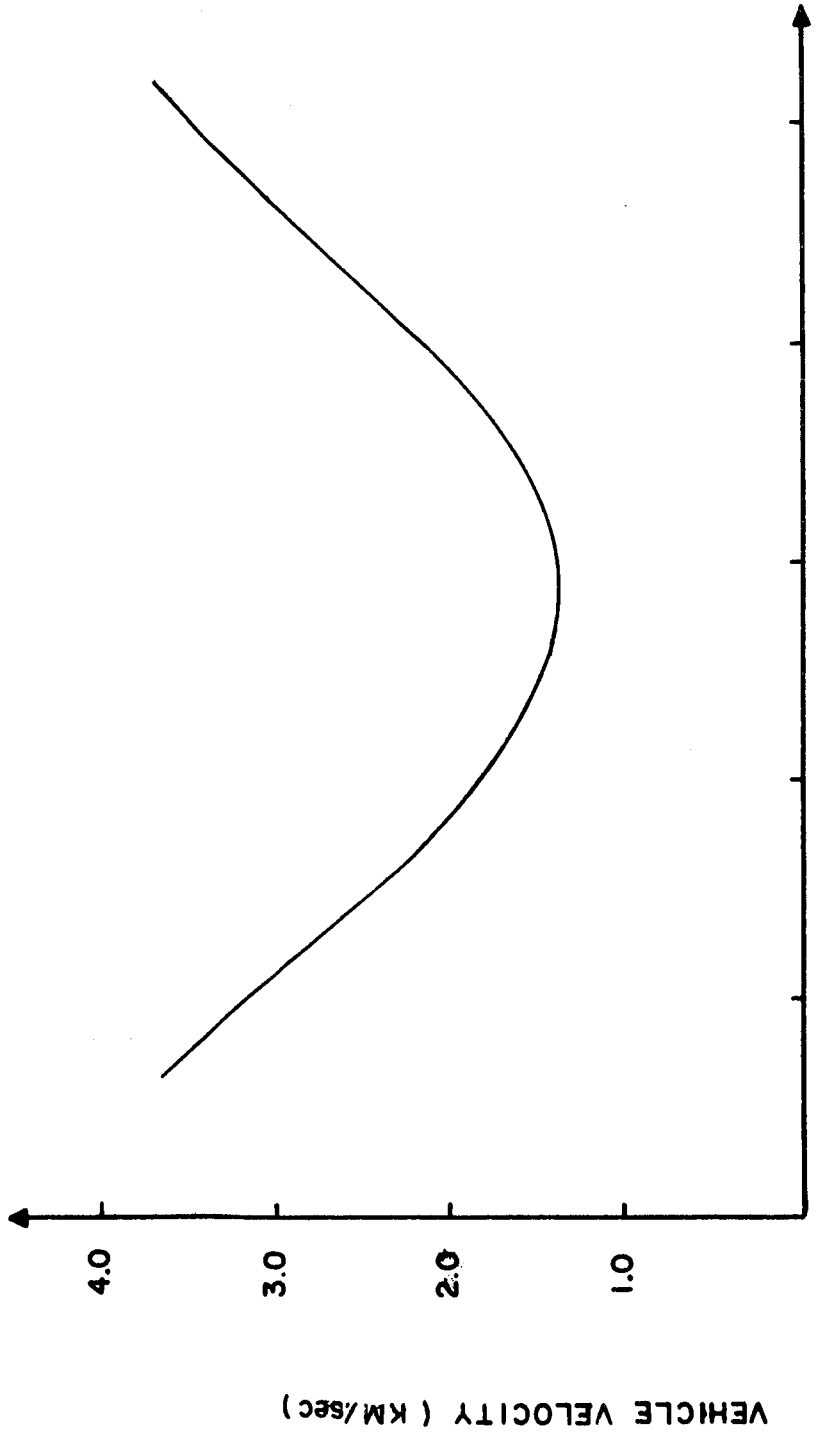

TOTAL VEHICLE VELOCITY

FIGURE 14

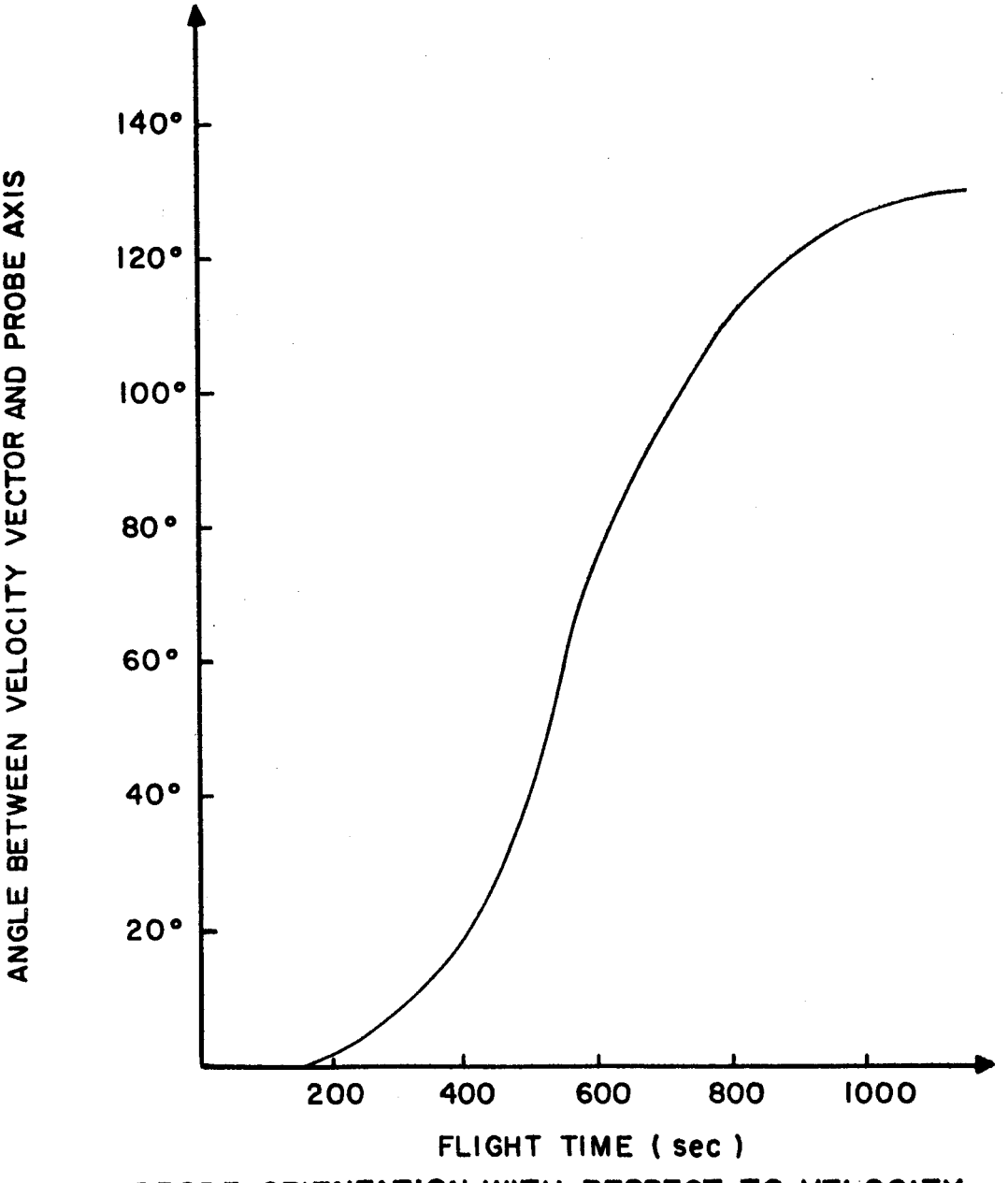

PROBE ORIENTATION WITH RESPECT TO VELOCITY VECTOR

FIGURE 15

angle θ between the velocity vector and the probe axis varied during the flight. The angle information was obtained by analyzing magnetometer data to determine the attitude of the probe; the direction of the velocity vector was known from radar data.

Typical telemetry data is shown in Figure 16, where positive current is represented by a downward displacement. The lower curve is the sweep voltage which has been drawn over representative points which were obtained from a commutated telemetry channel.

The reduced ion current data yielded the profile shown in Figure 17. Electron densities as determined by the Mother-Daughter technique, simultaneous ionosonde from Wallops Island, and Alouette topside sounder data are also shown for comparison.

3.1.1 Spin Modulation of the Current

Current oscillations as shown in Figure 16 were exhibited throughout the flight and the frequency of these oscillations corresponded exactly to the spin rate of the rocket as determined from solar aspect sensor data. The probe was mounted on the top of the payload in a cylindrical aluminum housing next to a center post with a magnetometer on the other side of the center post. The probe mounting with its pertinent dimensions is illustrated in Figure 18. A center post disturbance probably caused current oscillations as the probe rotated under its influence. The attitude of the payload was 26° from the vertical and did not vary by more than $\pm 2^{\circ}$ while ion current measurements were being made.

The per cent oscillation versus flight time is shown in Figure 19. The initial rapidly-decreasing oscillation may be due to

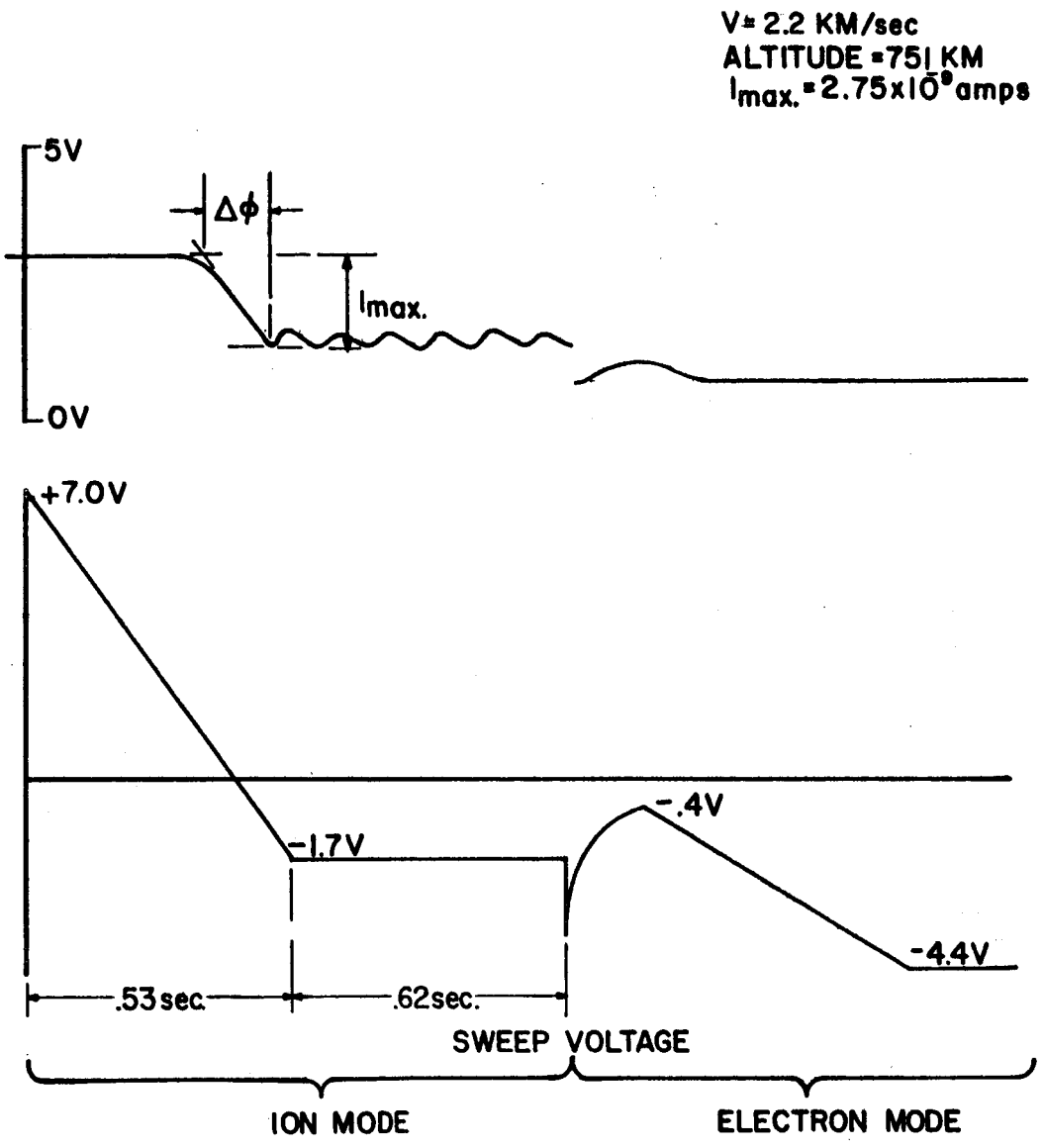

TYPICAL TELEMETRY DATA

FIGURE 16

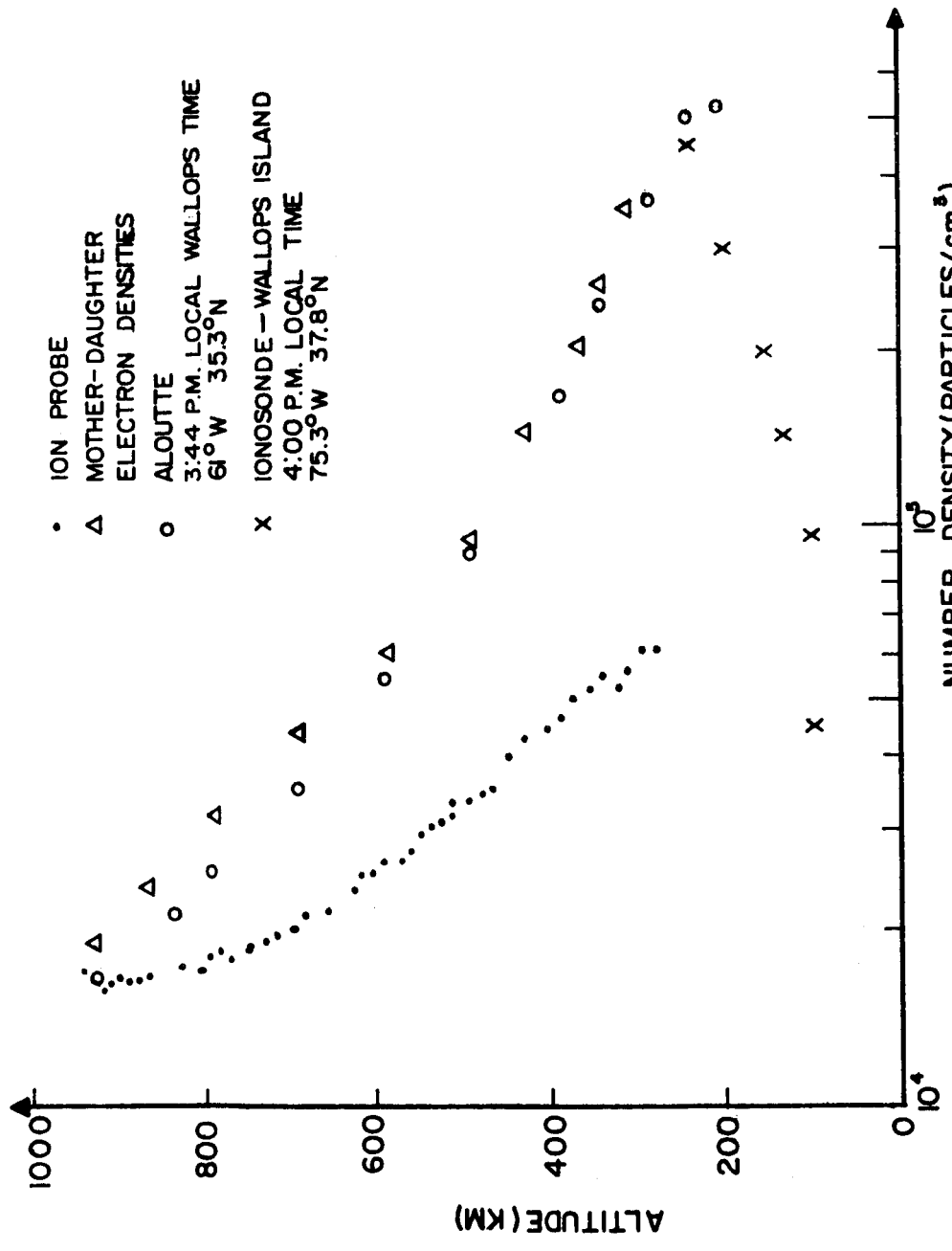

ION DENSITY PROFILE

FIGURE 17

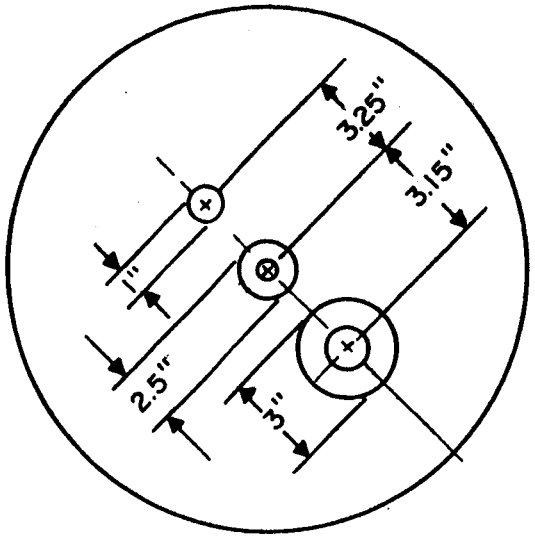

TOP VIEW

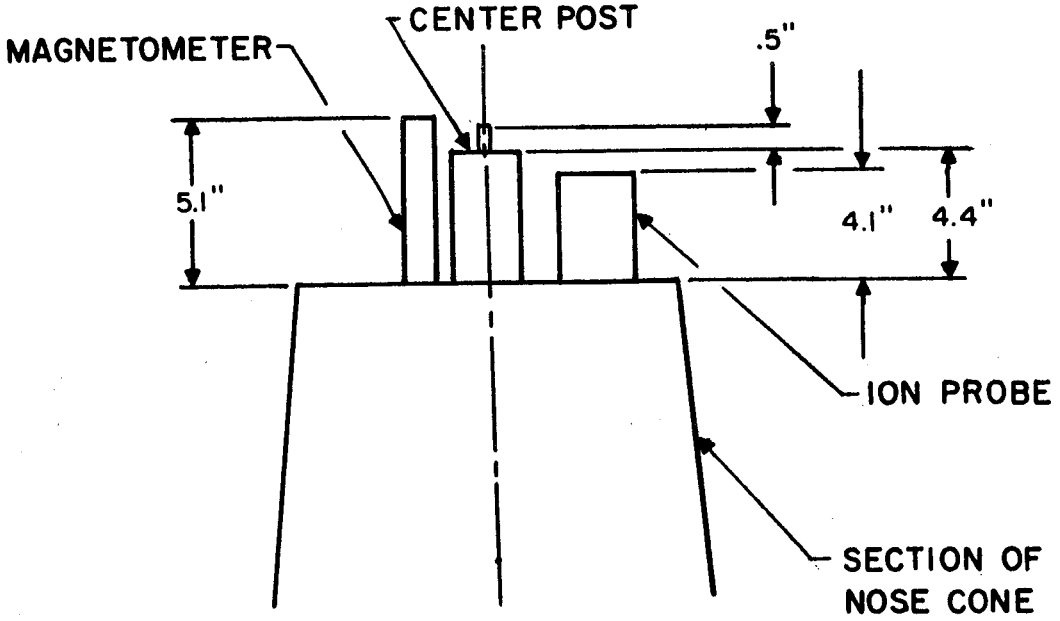

SIDE VIEW

PROBE MOUNTING

FIGURE 18

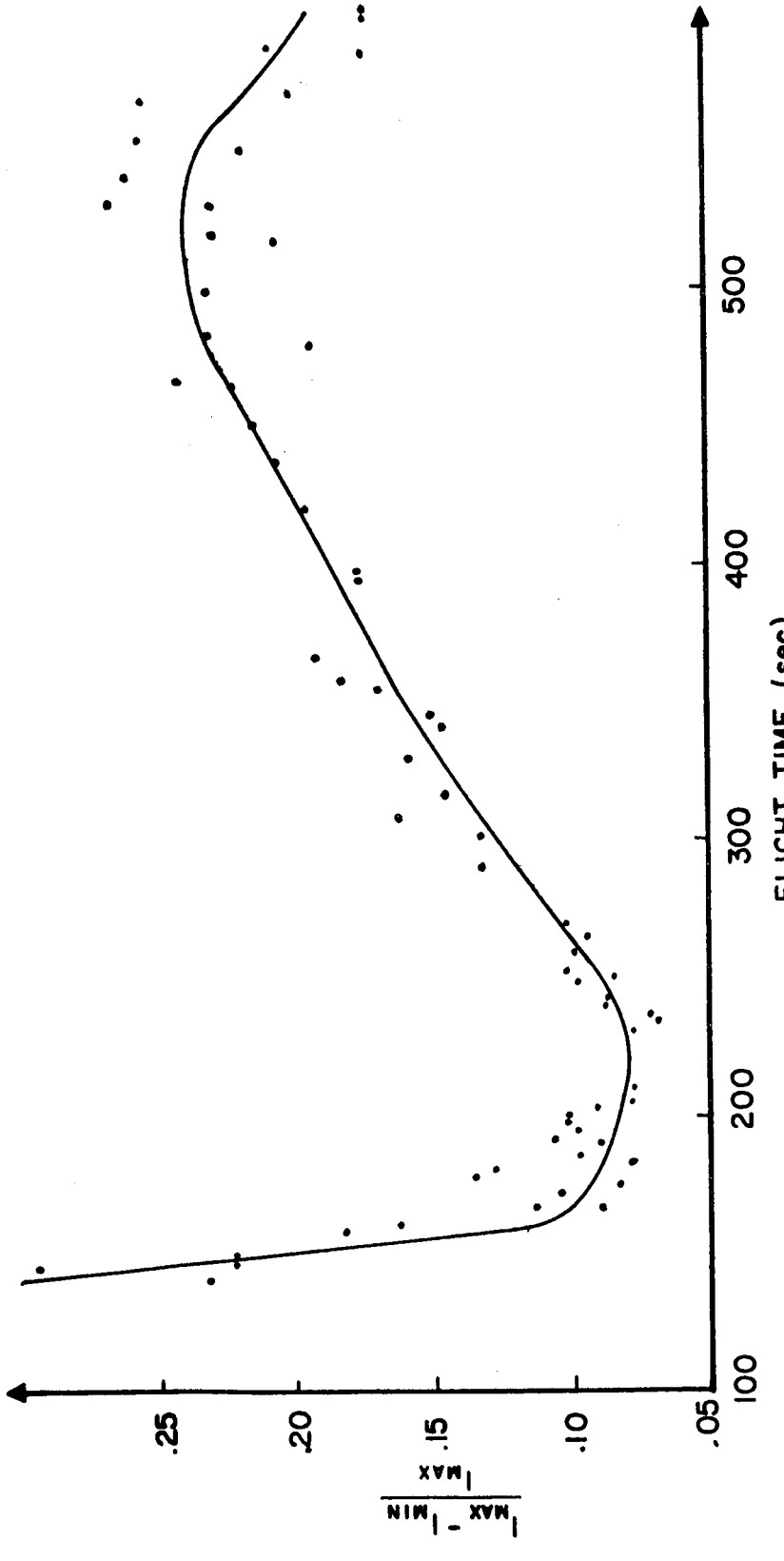
PER CENT CURRENT OSCILLATIONS
$\frac{I_{MAX} - I_{MIN}}{I_{MAX}}$
.25
.20
.15
.10
.05
100
200
300
400
500
FLIGHT TIME (sec)

FIGURE 19

the wake of the leading payload section (the nose cone separated into two sections at 139 sec in the flight) as the probe rotated in its wake. The Mach cone angle was calculated to be approximately 25° corresponding to experimental conditions at a height of 300 km so that the ion probe was definitely in the wake of the other nose cone section during this part of the flight.

The increase of oscillations during the remainder of the ascent may be explained in the following manner: the direction of the velocity vector is slowly becoming more horizontal so that the collected ions are being swept in from a more horizontal direction under the influence of the center post.

Solar aspect sensor data was used to check this hypothesis and the results were encouraging. As shown in Figure 20, it was found that the current maximums occurred when the probe was 14° from the leading edge of the payload, and the current minimums occurred when the probe was approximately 23° from being directly behind the magnetometer and center post with respect to the horizontal component of velocity which was 7° south of east. The estimated accuracy of these measurements is $\pm 10^{\circ}$, and they are reasonably consistent with the expected result that minimum current was collected when the ion probe was obstructed by the center post by a wake and/or electric field mechanism.

It seems likely that the electric field in the vicinity of the probe and the center post contributed to the observed results. Because of the rotation of the probe, not all the collected ions passed through an identical electric field with the result being variations in the current level as the probe rotated.

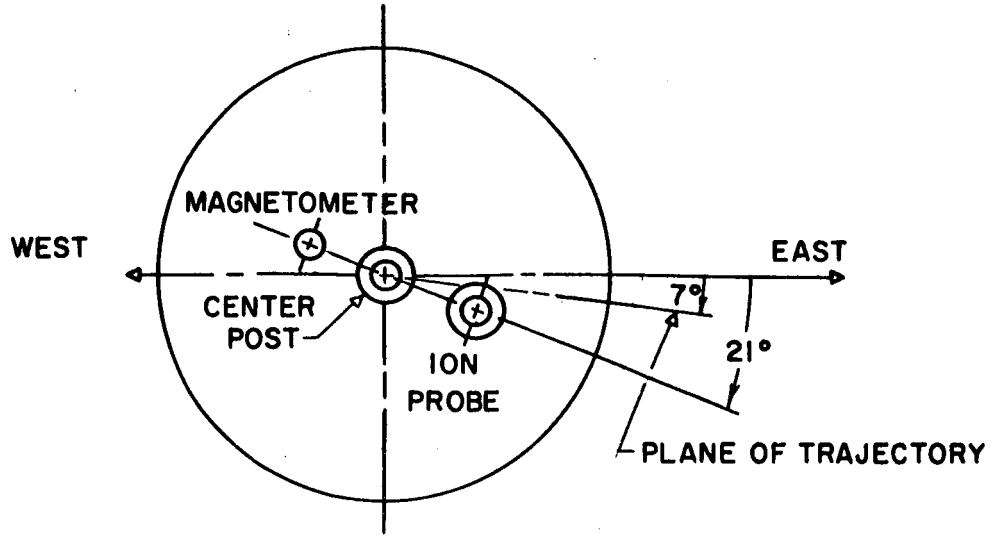

PROBE ORIENTATION AT TIME OF I_{MAX}

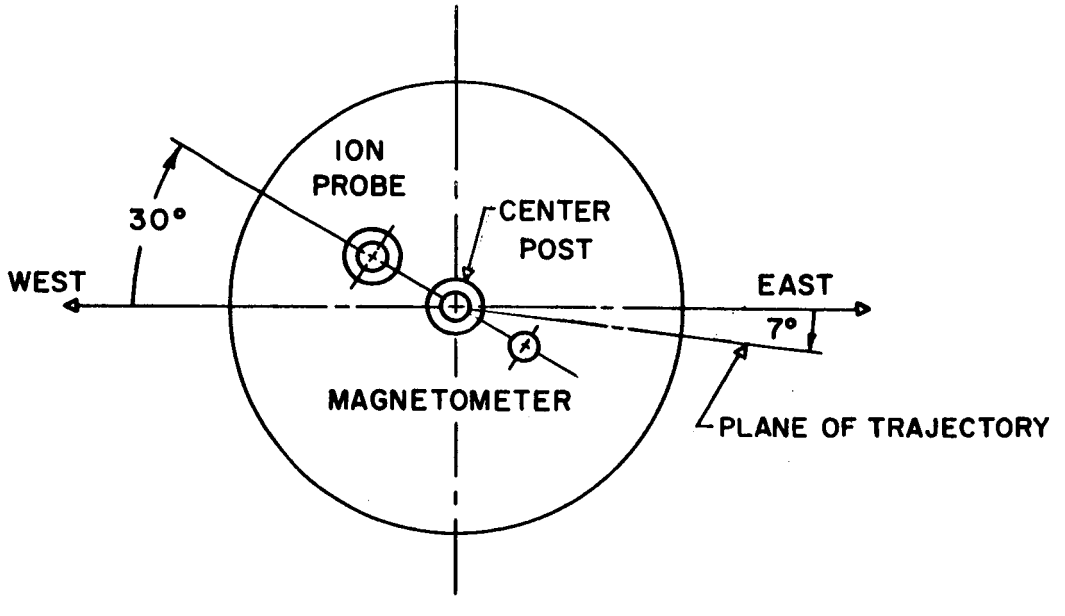

PROBE ORIENTATION AT TIME OF I_{MIN}

PROBE ORIENTATION AT TIME OF I_{MAX} AND I_{MIN}

FIGURE 20

3.1.2 Scale Height

The ion scale height H_i depends on the sum of ion and electron temperature as shown in equation 3.2 for diffusive equilibrium.

$$-\frac{d}{dz} \log_e N(z) = \frac{gm_i}{k(T_e + T_i)} = \frac{1}{H_i} \qquad (3.2)$$

$N(z)$, m_i, and g are respectively the charged particle density, average ion mass, and acceleration of gravity at the altitude z, while T_e and T_i are the electron and positive ion temperatures.

At 600 km the calculated scale height was 274 km, yielding an effective charged particle temperature, $\frac{T_e + T_i}{2}$, of 2160° K, assuming only O^+ ions to be present. In these calculations data obtained from the Mother-Daughter profile was used because the measured ion profile was obviously in error,

$$N(625 \text{ km}) = 5.45 \times 10^4 \text{ electrons/cm}^3 ,$$

$$N(575 \text{ km}) = 6.54 \times 10^4 \text{ electrons/cm}^3 ,$$

while $g(600 \text{ km}) = 8.16 \text{ m/sec}^2$.

The scale height was determined at an altitude of 600 km because at lower altitudes the slope of the Mother-Daughter profile is not constant.

Since there is an absence of thermal equilibrium during the daytime (Bauer and Blumle, 1964) with T_e/T_i estimated at 1.5 at 600 km, the inferred ion temperature is 1730° K.

3.2 Vehicle Potential

As a vehicle traverses the ionosphere, it acquires a potential due to the presence of charged particles, and this potential is usually negative due to the larger thermal velocities of electrons.

The outer grid of the probe was tied to vehicle ground so that the total potential, ϕ_t, was the sum of the vehicle potential and the retarding grid potential.

$$\phi_t = \phi_g + \phi_v \tag{3.3}$$

ϕ_v is the vehicle potential with respect to the plasma and ϕ_g is the grid sweep voltage.

If ϕ_o is defined as the sweep voltage which is just sufficient to repel ions which have a zero velocity component (in the earth's reference frame) in the direction of the vehicle velocity vector, then vehicle potential is given by

$$\phi_v = \frac{1}{2}\frac{m}{e}(V \cos\theta)^2 - \phi_o \quad . \tag{3.4}$$

ϕ_o was determined at the point $I = I_{max}/2$, which causes only a slight overestimate of the negative potential provided $V \cos\theta >> a$.

The calculated vehicle potentials are shown in Figure 21. Vehicle potential varied only slightly throughout the ascent and had an average value of -2.3 volts. The calculated potentials were high, and this was partly because the rocket velocity was not much greater than the most probable ion velocity.

When

$$e\phi_t = \frac{1}{2}m(V \cos\theta)^2 \quad , \tag{3.5}$$

then $x = o$, and the current is

$$I = \alpha eAN\left(\frac{V \cos\theta}{2} + \frac{a}{2\sqrt{\pi}}\right) \quad , \tag{3.6}$$

which for large $V \cos\theta / a$ approaches one half the maximum current.

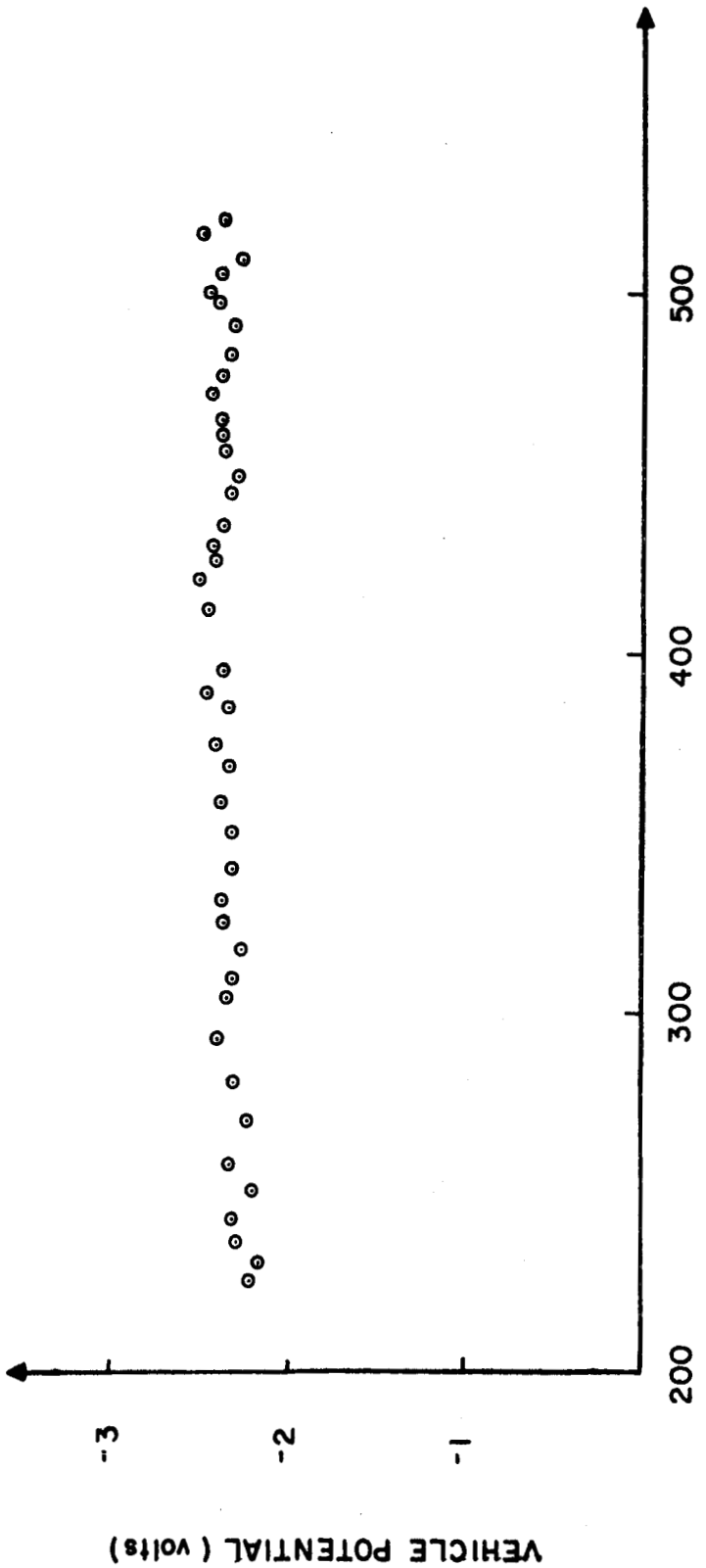
VEHICLE POTENTIAL (volts)
-3
-2
-1
200
300
400
500
FLIGHT TIME (sec)
VEHICLE POTENTIAL

FIGURE 21

But throughout the flight, the $V \cos\theta / a$ ratio varied from only 3 down to less than 1. As a typical example, at 600 km, $V \cos\theta / a \simeq 2$ and it was determined from equation 3.6 and the telemetry data that this low value of the $V \cos\theta / a$ ratio caused an overestimate of the negative vehicle potential by .4 volts. Considering this source of error, the average vehicle potential would be -1.9 volts.

Contact potential can be significant and should be considered in determining vehicle potential. With the aid of laboratory calibrations, using an ion source and test chamber, Anderson and Bennett (1965) found a contact potential of .5 volts existed between the aluminum skin of a vehicle and the retarding grid doublet. The magnitude of this effect will depend upon the types of metals used.

Tungsten has a work function between 4 and 5 electron volts and aluminum has a lower work function between 3 and 4 volts. If tungsten and aluminum are brought into electrical contact, tungsten will have a negative potential with respect to the aluminum. This potential will equal the difference in the work functions and will depend on the surface conditions of the metals.

Because work functions are dependent upon surface conditions, only an estimate of this effect is possible. But, it is obvious that the contact potential between the tungsten grids and the aluminum housing caused the calculated vehicle potential to be more negative, and this effect can be of the order of .5 to 1 volts.

3.3 Ion Temperature

Ion temperature can be estimated from equation 2.12. Around $x = o$, $\frac{dI}{d\phi}$ has a maximum negative value which corresponds to approximately half the ions being collected at the region half way

down the ϕ-I characteristics. Near x = o,

$$e\phi \simeq \frac{1}{2} m (V \cos\theta)^2 \quad , \tag{3.7}$$

$$a = \sqrt{2kT/m} \quad , \tag{3.8}$$

and after substituting for ϕ, a, and x, equation 2.12 reduces to

$$\frac{dI}{d\phi} = \frac{-\alpha e^2 AN}{\sqrt{2kT\pi m}} \quad . \tag{3.9}$$

Equation 3.9 can be solved for ion temperature, yielding

$$T \simeq \frac{e^2}{2\pi km} \left(\frac{I_{max}}{V \cos\theta \left(\frac{dI}{d\phi}\right)_{max}}\right)^2 \quad . \tag{3.10}$$

$\Delta\phi$ is defined as the total change in grid potential that takes place while the collector current increases from zero to its maximum value at its maximum rate of increase.

$$\Delta\phi = \frac{I_{max}}{\left(\frac{dI}{d\phi}\right)_{max}} \tag{3.11}$$

Then, ion temperature reduces to

$$T \simeq 1.11 \times 10^{10} \left(\frac{\Delta\phi}{V \cos\theta}\right)^2 \quad . \tag{3.12}$$

In equation 3.12 it is assumed that only atomic oxygen ions are collected. $\Delta\phi$ is as shown in Figure 16, and the dimensions of V are m/sec.

From Figure 4, it is seen that $\frac{dI}{d\phi}$ changes very rapidly on either side of the maximum. This is a major source of error in determining ion temperature, especially since any error in $\frac{dI}{d\phi}$ will be squared.

A sample of the calculated ion temperatures is presented in Figure 22. The results are erratic and generally lie in a range from 2000 to 4000° K, with a few points being even higher than 4000° K. The average ion temperature below 900 km is 3300° K.

3.4 Electron Temperature

A measurable electron current was not collected during the electron mode as can be seen in Figure 16. Thus, no electron temperature calculations could be made.

In any subsequent experimental work, the current sensitivity in the electron mode will need to be increased if electron measurements are to be made. The high negative potential, -1.9 volts, kept the electron flux to the probe lower than anticipated and this is the reason why the instrument sensitivity in the electron mode was not sufficient for the experimental objectives.

3.5 Derivative Channel

The output of the derivative channel exceeded the 0 to 5 volt limits of telemetry so that the waveforms resembled the curves of Figure 7, except that the upper portions of the curves were chopped off. The time constants of Figure 7, $\tau_1 = .059$ sec and $\tau_2 = .0015$ sec, were the values used for the flight instrument.

About the only measurable quantity was the pulse width at some arbitrary level, but as can be seen from Figure 7, pulse width remains fairly constant even though the plasma composition varies. Thus, no useful ion composition information was obtained from the derivative data.

Naturally, the spin modulation of the current appeared differentiated on the derivative channel and this distortion of the

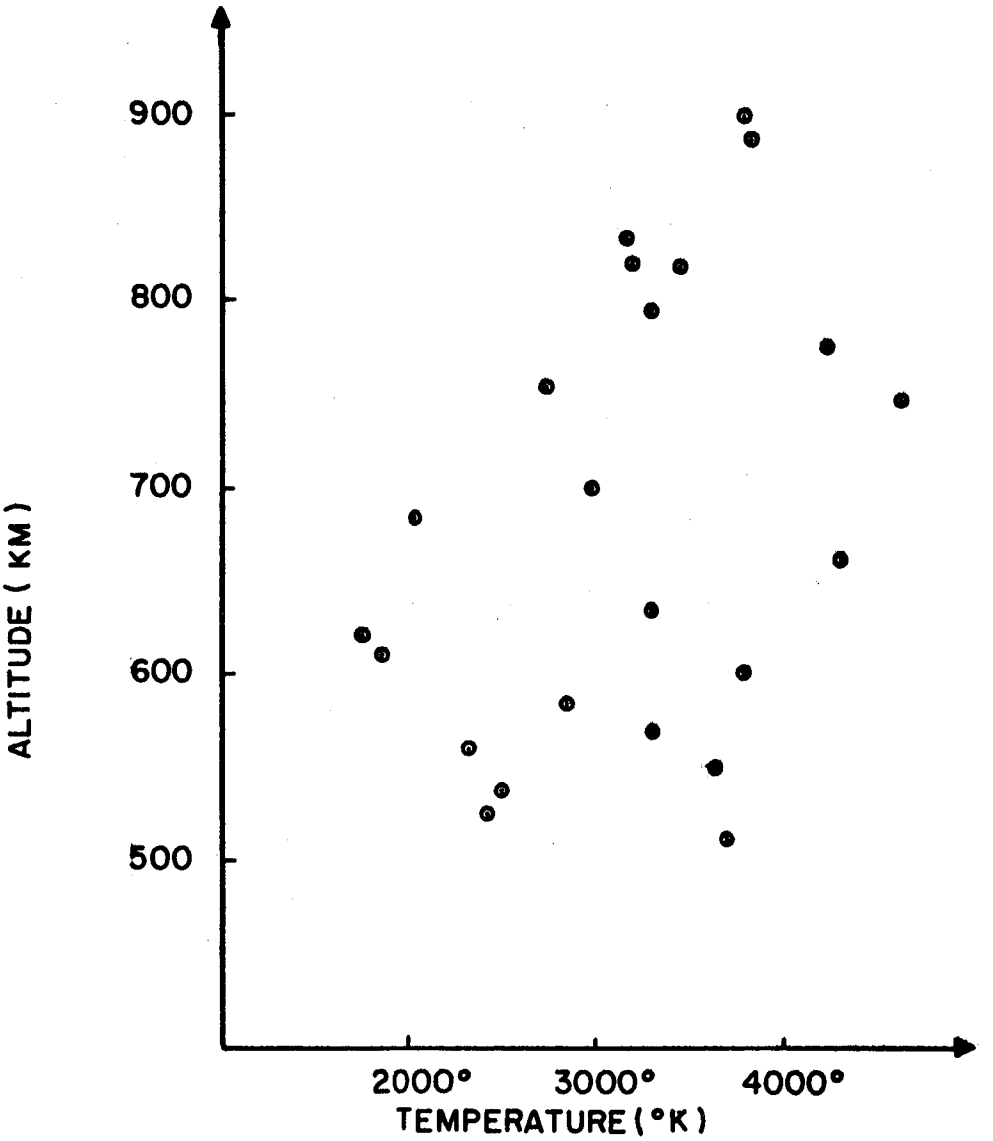

ION TEMPERATURES

FIGURE 22

derivative characteristics reduced the quality of this data.

IV. CONSIDERATIONS AND DISCUSSION

4.1 Ion Composition

From the analysis of the differentiating circuit for the various time constants, it is seen that a comparison of experimental and theoretical derivative characteristics could be employed to determine the ionic constituents. Because of the more distinctive features of the derivative characteristics, such as variations in amplitude and shape, the derivative method would be slightly more accurate than comparing current characteristics. However, the increased accuracy would be relatively minor so that no significant advances in the field of ion composition measurements would result.

There were no salient features of derivative characteristics (Figures 6 - 11) which suggested a new approach to the problem of determining ion composition.

Because the spin modulation of the current caused considerable variations in the shape of the probe characteristics, no effort was made to compare or obtain the best fit of theoretical characteristics to experimental results. Consequently, ion composition was not determined.

4.2 Ion Density Profile

As seen from Figure 17, the calculated ion densities are low as compared to ionosonde data and Mother-Daughter results. It is estimated that the experimental error is ±20% for this type of experiment, but this does not account for the large discrepancies of Figure 17. The ion probe results are incorrect by approximately a factor of four at the lower altitudes since the ionosonde data is most probably accurate to within 5%.

There are three distinct regions in the profile of Figure 17. For altitudes below 450 km, the ion probe results are extremely low. From approximately 450 to 700 km, the error in the ion probe results is fairly constant, assuming the Mother-Daughter profile is correct. Above 700 km, the ion densities are decreasing more slowly with altitude and approach the densities measured by the Mother-Daughter method. The ion profile will be explained in terms of these three regions.

The possibility that a wake effect might have caused the exceptionally poor results at the altitudes below approximately 450 km was investigated. The nose cone separated into two sections at 139 sec in the flight and the probe was in the wake of the leading payload section during the critical period when a comparison with ionosonde data would normally be applicable. This wake effect would be decreasing as the distance between the two sections increased, and the two sections were moving away from each other with a relative velocity of 5. 34 m/sec after separation.

A wake effect could easily explain the large error during the critical period just after separation when the separation distance was not great. Samir and Willmore (1965) have studied these effects experimentally and their results show that there is a wake strongly depleted of ions and electrons due to supersonic bodies moving through the ionsophere. However, 40 seconds after separation, the payload sections were already more than 200 m apart. Thus, it is improbable that the wake of leading payload section could have caused the low ion density measurements which were obtained during the remainder of the flight.

If it is accepted that low ion densities were caused by a wake depleted of ions, then why were not the electron densities as measured by the Mother-Daughter experiment also reduced so as to maintain electrical neutrality of the plasma? The Mother-Daughter technique involved propagation with antennas of fairly wide beam width so that the rf transmission path may not have been primarily line of sight between the two payload sections and in the wake. Then, the effects of the wake might not be observable on the electron density profile.

Between 450 and 700 km, the ion densities of Figure 17 are consistently low, but the slope of the profile is nearly correct. It is believed that the low densities are due to an inaccurate geometrical determination of the transmission coefficient, α_1, of a single grid. Theoretically, α_1 was found to be .93 by determining the fraction of the area which was unobstructed by the grid wires, but this was probably an overestimate of α_1.

Hanson et al. (1964) measured the transparency of their grids at about 87%. Geometrically, the transparency would have been about 97% and this would have been an overestimate of α_1 by 12%. In an earlier experiment by Hanson and McKibben (1961), a theoretical value of α_1 would have been higher than the actual value by 15%; a transmission coefficient of .56 was measured for 3 planar grids of 1 mil wire with approximately a 1 mm mesh dimension. Extrapolated to 4 grids, this low a value of α would explain the discrepancy in the ion profile of Figure 17 at the middle altitudes. The instrumentation used by Hanson was of the same size wire, with approximately the same per cent area obstructed by the wire (within

about 5% per grid) so that a comparison is valid. Because of these facts, there can be little doubt that the correction of α to a lower value is justified.

A difference between theoretical and true values of α_1 of the order described would result in a considerably larger error in the total transmission coefficient for 4 grids and would be sufficient to correct the ion density profile of Figure 17. The normalized profile of Figure 23 corresponds to the assumption that under experimental conditions, α_1 was .78 instead of the theoretically determined value of .93 and in view of the examples from the literature, this is a reasonable estimate of the correct value. Appendix B describes some pertinent laboratory measurements of the optical transparency of grids.

Above 700 km, the calculated densities of Figure 23 are high and indicate that more current was collected than the simplified ram theory of equation 3.1 predicted. This was expected since ion densities, obtained either when the ion thermal velocity approaches the velocity of the vehicle or when planar traps are pointed at too large an angle from the velocity vector, have been too high (Bourdeau, 1963). Both these conditions occurred near apogee of this vertical sounding rocket. However, the amount of error due to these factors should have been considerably less than the observed errors.

Calculations were made, using the complete current expression, equation 4.1, to determine exactly how accurate the approximation, $I = \alpha eANV \cos\theta$, was at the lower velocities and larger angles of attack,

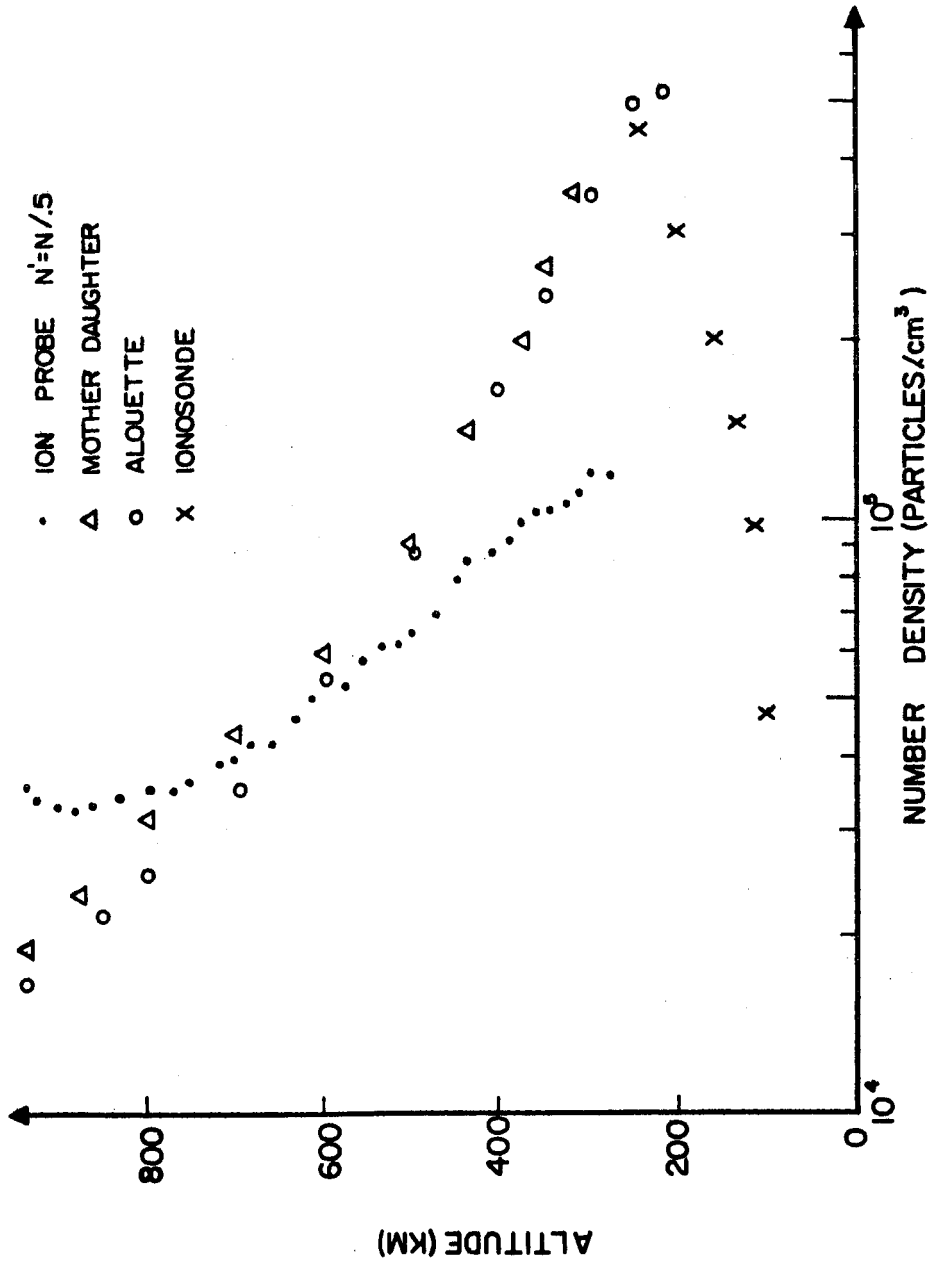

NORMALIZED ION DENSITY PROFILE

FIGURE 23

$$I = \alpha eANV \cos\theta \left(\frac{1}{2} + \frac{1}{2}\mathrm{erf}(x) + \frac{e^{-x^2}}{2x\sqrt{\pi}}\right) , \qquad (4.1)$$

where $x = \frac{V \cos\theta}{a}$ at $\phi_t = 0$. At an altitude of 910 km, the He^+ and H^+ concentrations were assumed to be 10% and 5% of the total positive ion composition, consistent with He^+ and H^+ concentrations determined by Taylor et al. (1963) by means of a ion mass spectrometer. For a temperature of 1730° K, the calculations showed that any error in the measured densities resulting from using the approximate equation was less than 3%. Thus, the high densities cannot be explained by the theory of equation 4.1.

The data also revealed that a relatively large current was collected during descent as illustrated in Figure 24. These currents are in agreement with data obtained by Samir and Willmore (1965) who also collected a significant fraction of the ambient density in the wake.

For an accurate calculation of the wake current, an analysis taking into account vehicle potential is needed. However, it is usually assumed that the electric field is small so that the ion flux can be approximated by the neutral particle flux. Applying this assumption, Samir and Willmore concluded that the experimental wake currents were much higher than could be explained by considering only the thermal motion of the ions. This is also true of the currents illustrated in Figure 24 and was verified by making the necessary calculations. Equation 4.1 was employed but one must be careful to use the proper signs for angles of attack larger than 90°. This equation was also derived by Al'Pert et al. (1963) for neutral particles collected in the wake of a sphere.

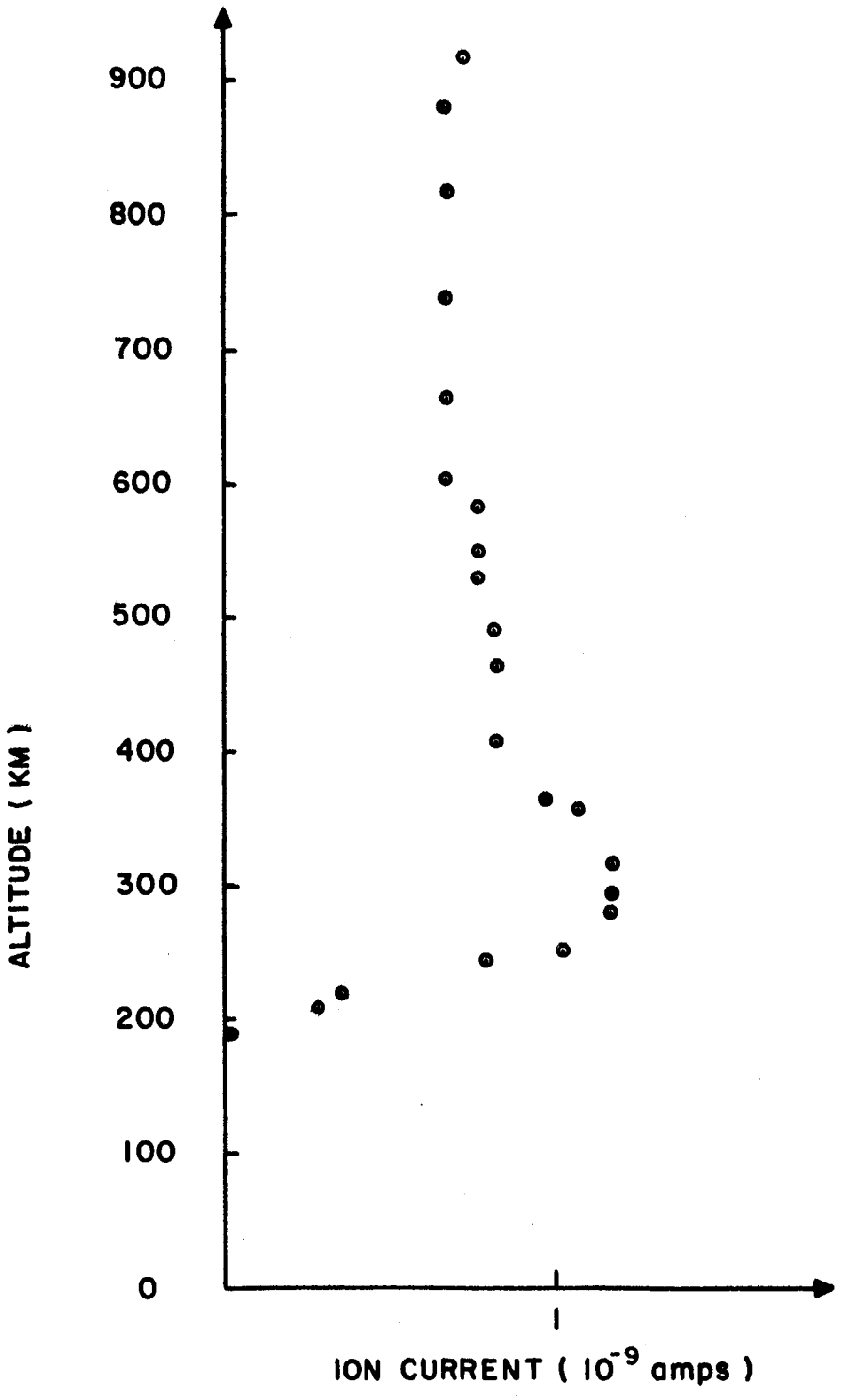

CURRENT COLLECTED DURING DESCENT

FIGURE 24

Since an unexplained current was collected during descent, it seemed likely that this effect would also have been present during ascent. If this is correct, the descent current should be a reasonable indication of the amount of excess ascent current which was not accounted for by the theory. Thus, a corrected profile was obtained by subtracting the descent from the ascent current before calculating the normalized densities. The resultant corrected profile of Figure 25 agrees fairly well with the Mother-Daughter results except at the lowest altitudes.

The problem is to determine what mechanism caused the current of approximately $.7 \times 10^{-9}$ amps which was collected during descent.

This was not a photoelectric effect since a large negative voltage on grid G_4 suppressed local electrons. In addition, the angle between the sun and the probe axis was about 95^{o}. Also, from Figure 24, it is seen that the effect is related to the ambient ion density, judging from the way the current peaked just above the F peak.

A plausible explanation seems to be that the negative vehicle potential of -1.9 volts attracted and collected ions that would otherwise not have been collected. This would cause an increase in the effective collection area.

Sagalyn et al. (1963) took into account the effects of vehicle potential on their spherical electrostatic analyzer by determining experimentally from the flight data an $f(\phi)$ function which was defined as

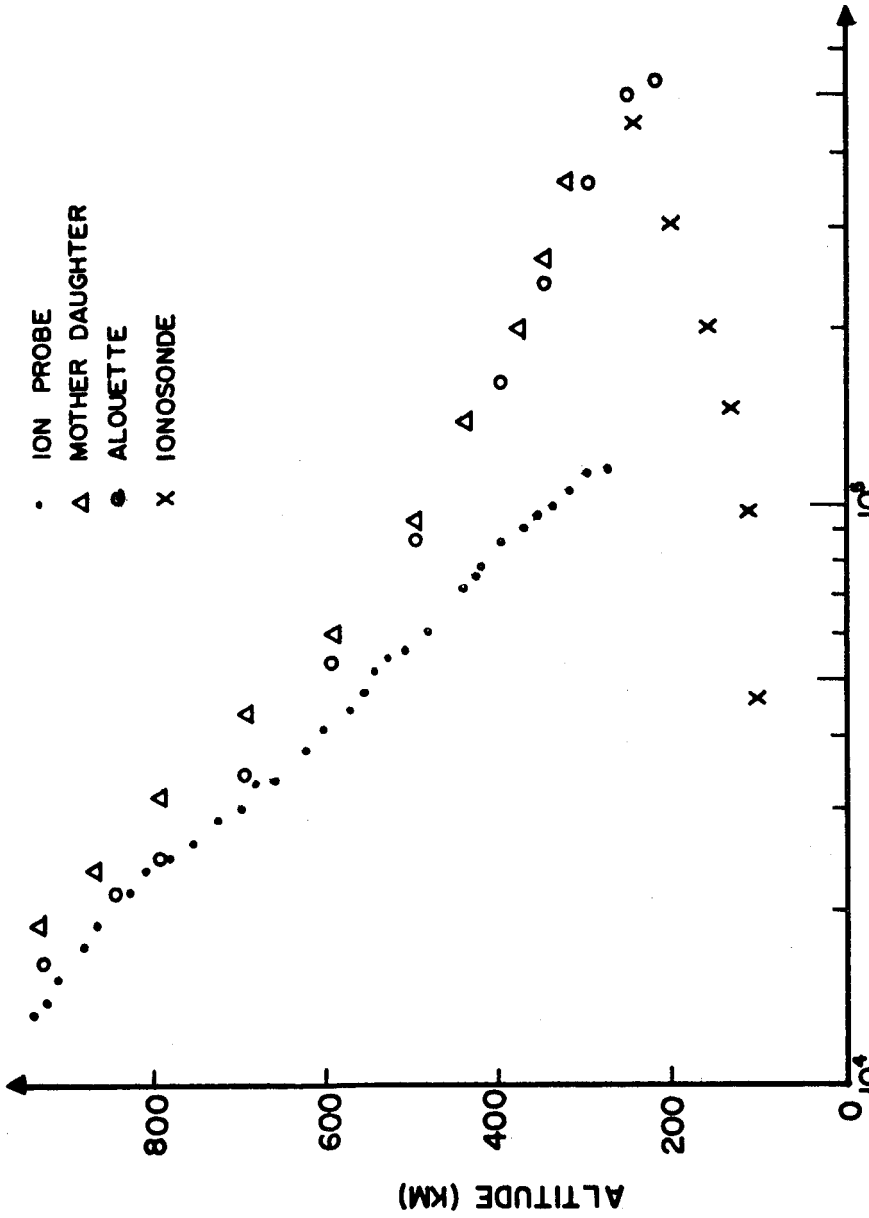

NORMALIZED PROFILE CORRECTED FOR DESCENT CURRENT

FIGURE 25

$$f(\phi) = \frac{I_o}{I_{-\phi_v}} \quad , \tag{4.2}$$

where I_o and $I_{-\phi_v}$ are the currents measured at $\phi_g = 0$ and $\phi_g = -\phi_v$. In other words, the densities were not determined from the maximum current but from the current collected when the total potential was zero. It seems logical that this reasoning would be at least partially applicable to the present problem at least as a method of estimating the effects of the electric field.

Sagalyn et al. reported an $f(\phi)$ of 1.45 at $\phi_v = -1.7$ volts while this experiment yielded an $f(\phi)$ of 1.6 at $\phi_v = -1.9$ volts for the higher altitudes and decreased to about 1.1 at the lower altitudes. An $f(\phi)$ of this nature would be consistent with the corrections needed to improve the accuracy of the profile. A larger $f(\phi)$ near apogee would reduce the high calculated densities, and as $f(\phi)$ approaches 1 at the lower altitudes, the correction would become negligible.

It is of interest to note that other experimenters have obtained ionospheric data which could not be interpreted in an entirely consistent manner.

An investigation of the ionic composition of the atmosphere was performed by Istomin (1963) with a radio-frequency mass spectrometer. During descent, while the instrument was in the "shadow cone", a considerable number of O^+ ions were collected. Istomin concluded that the observed phenomenon could be accounted for either by O^+ drift velocities of the order of 1 km/sec, or by very high velocities of random motion requiring half of the O^+ ions at a height of 250 km to have temperatures of at least $20,000^{\circ}$ K. Several mechanisms by which "hot" ions can be produced were presented.

Both of these hypothetical phenomena were rejected as possible explanations of the data presented in this analysis since their existence is completely at variance with our present understanding of the ionosphere.

4.3 Sheath Thickness Effects

In order to check the accuracy of the method of analysis employed (that is the use of the equations derived by Whipple), the case where the angle of attack was 90° was investigated. Then, $V \cos\theta = 0$ and, for an attracting field, the current reduces to the well known equation for the thermal current to a stationary probe.

$$I = \frac{\alpha e A N a}{2\sqrt{\pi}} \qquad (4.3)$$

From equation 4.3, the current was found to be $.3 \times 10^{-9}$ amps for an ion temperature of 1730° K and density of 1.7×10^{4} ions/cm^3, assuming the plasma composition to be 5% H^+, 10% He^+ and 85% O^+. This calculated value is approximately half the measured value of $.67 \times 10^{-9}$ amps which was obtained during descent near 900 km, when $\theta = 90^{\circ}$.

It appears there must be an additional process by which ions are collected. From a consideration of the physics involved, it is seen that there is a current due to the edge effects of the electric field in the sheath region. These currents are illustrated in Figure 26, which is an extremely simplified model and only one special case of the more difficult problem for intermediate angles of attack. Because of the complexity of the problem, only an approximation of the excess current due to the electric field could be made. Since the sheath thickness was approximately 12 cm,

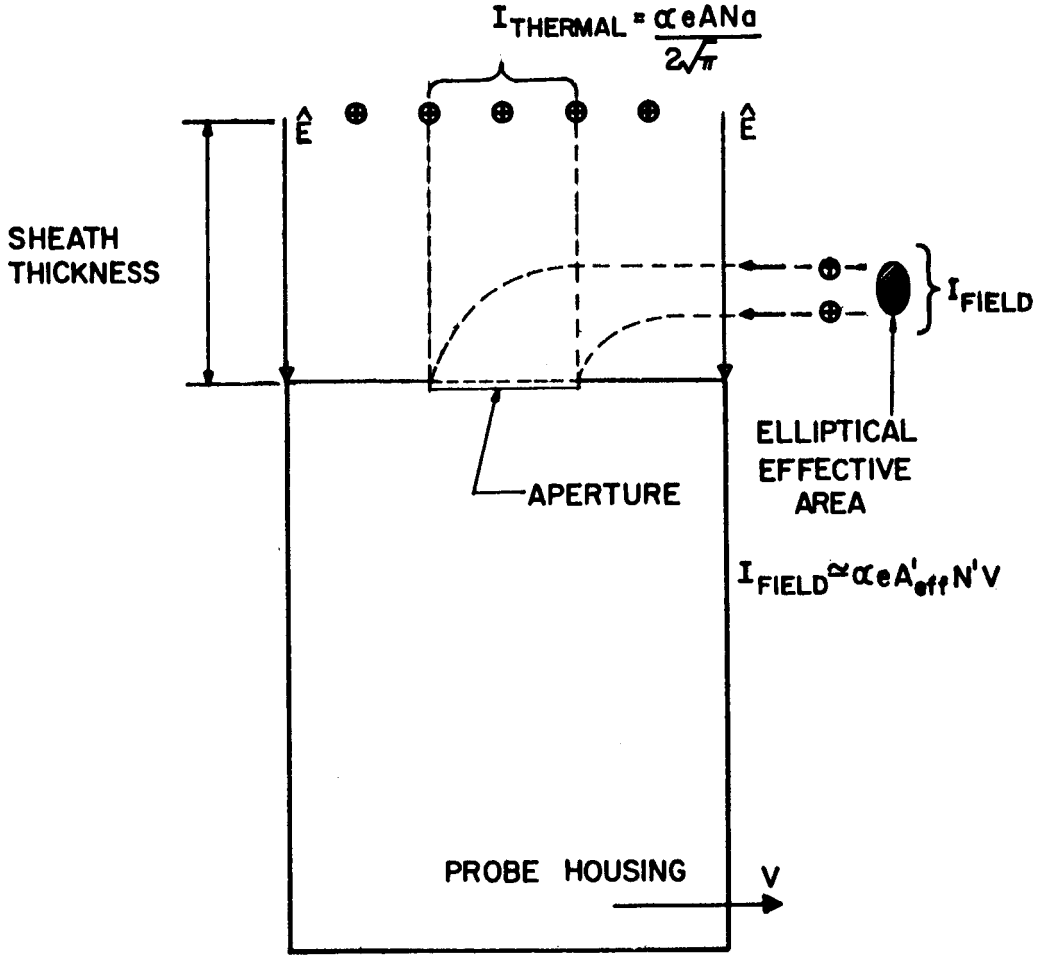

ION CURRENTS DUE TO THERMAL MOTION AND ELECTRIC FIELD FORCES

FIGURE 26

ions at greater distances were not collected.

The significance of the Debye length is that any shielding of a charged body by space charge in the surrounding plasma occurs in a distance of the order of a Debye length, L, where,

$$L = \sqrt{\varepsilon_o kT/Ne^2} \qquad (4.4)$$

and ε_o is the permittivity. For T = 1730° K, and N = 1.7 x 10^4 ions/cm^3, the Debye length would be 2 cm. The parameters used in the trajectory analysis were:

sheath thickness, S, = 12 cm

ϕ = -1.4 volts (estimated vehicle potential if a contact potential of .5 volts is assumed)

V = 1.5 km/sec

N = 1.7 x 10^4 ions/cm^3

The electric field was considered uniform and was found from $E = \phi/S$ and only the field directly above the metalic probe surface was considered (fringing of the field was neglected).

From the trajectory calculations, an effective collector area was found, even though the projected collector area in the direction of the velocity vector was zero. This effective area would cause a current of the correct order of magnitude to explain the difference between the measured wake current of .67 x 10^{-9} amps and the theoretical thermal current of .3 x 10^{-9} amps.

This analysis indicates that Whipple's results need to be supplemented with equations which take into account the potential and physical dimensions of the instrument. A general analysis cannot be presented since the field will depend on the size and shape

of a particular probe configuration, and on the characteristics of the plasma in a non-linear manner. Whipple's equations are valid for a collector mounted on an infinite plane, but when finite dimensions are considered, they do not include all ion collection mechanisms.

The trajectory analysis was applied for an intermediate angle of attack at $\theta = 40^{\circ}$. The calculations showed that for particle velocities of the order of the mean thermal velocities, some extra ions will be collected by the field effect, depending on the assumed velocity directions of the particles. It had been hoped that this current could be determined and then be applied as a correction to the ion density profile. But, the actual current, due to this mechanism, cannot be accurately calculated because of the complexity of the problem. However, this does demonstrate a method by which excess current was collected and is the most probable reason for the calculated densities being much too high near apogee.

When the sheath dimension becomes large compared to the probe, the electrical influence of the probe extends to a distance many times the probe dimension. This will tend to cause a focusing of the ions on the probe. The sheath thickness, S, can be estimated from equation 4.5 which was obtained by solving Poisson's equation for a planar geometry, assuming the charge density to be a constant value, Ne, for a distance S from the plane.

$$S = \sqrt{2e\phi/kT}\ L \qquad (4.5)$$

Jastrow and Pearse (1957) derived an identical expression for a

sphere when S is much less than R, where R was the radius of the sphere.

S was of the order of 12 cm at apogee and this means that the sheath thickness was comparable to the probe dimensions. Then, the potential in the sheath is important in determining the total collected current and Poisson's equation must be solved in the sheath with all sources of space charge being considered. This is an extremely complicated problem usually requiring numerical procedures.

Analysis of the situation was considered as part of a Doctorate thesis by Whipple (1965). He found it necessary to neglect the thermal motion of the ions, but the plasma temperature was taken into account through the Debye length. The ions were considered to be approaching the vehicle with a uniform speed from one direction .

This discussion simply points out the nature of the problems involved when the sheath dimension becomes of the order or larger than the probe dimensions. Theoretical studies by Whipple verify that this is a significant effect since he found that the ion current to a negatively-charged rapidly-moving sphere can be increased by at least a factor of 2 or 3 compared to the simple ram current.

It is evident that a solution for the probe configuration employed in this experiment (a plane collector mounted on a cylindrical housing) is a major undertaking beyond the scope of this analysis.

4.4 Ion Temperature

The computed ion temperatures of Figure 22 are higher

than more reasonable values obtained from scale height calculation. It is obvious that the current oscillations distorted the shape of the probe characteristics and caused considerable scatter in the calculated temperatures. Since ion temperatures are highly dependent upon accurately drawing a tangent to the maximum slope, which was distorted by the oscillations, the calculated ion temperatures are not as reliable as desired.

It has generally been the case that the direct measurement of ion temperatures by measuring the ion velocity distribution has yielded temperatures that were considered too high. It has been pointed out by Bourdeau (1963) that it is most likely that ion temperatures computed from planar ion traps are usually too high because the ion sheath is not planar. One of the factors disturbing the planar sheath was the contact potential difference between the outer tungsten grid and the aluminum housing.

V. SUMMARY AND CONCLUSIONS

5.1 Objectives of the Investigation

The purpose of this work was to obtain a direct measurement of ionospheric parameters using a retarding potential ion probe. The desired parameters were: positive ion density, composition, and temperature, electron temperature, and vehicle potential.

The derivative of the probe characteristics was investigated to determine if it would be useful in analyzing positive ion composition.

5.2 Review of the Procedure

The well known equation for ion current to retarding potential probe was used to determine positive ion density.

$$N = \frac{I_{max}}{\alpha e A V \cos\theta} \tag{5.1}$$

I_{max} was measured by the instrument when the total potential was such that no ions were being repelled. All other parameters were known so that an ion density profile was obtained.

Vehicle potential was determined from the equation,

$$\phi_v = \frac{1}{2}\frac{m}{e}(V\cos\theta)^2 - \phi_o \quad , \tag{5.2}$$

where ϕ_o was the sweep voltage at the point $I = I_{max}/2$.

Assuming that only atomic oxygen ions were collected, ion temperature was calculated from equation 5.3.

$$T = 1.11 \times 10^{10} \left(\frac{\Delta\phi}{V\cos\theta}\right)^2 \tag{5.3}$$

$\Delta\phi$ is defined as the total change in grid potential that occurs while the collector current increases from zero to its maximum value at its maximum rate of increase.

A conventional analysis of the differentiator was not used because of the complexity of the input function. Therefore, the convolution integral was used so that the differentiator output was approximated by

$$g(t) \simeq \sum_{n=-\infty}^{\infty} f(n\Delta\tau) \left(\frac{-c}{\tau_1 \tau_2} e^{-(t-n\Delta\tau)/\tau_1} + \frac{c}{\tau_2^2} e^{-(t-n\Delta\tau)/\tau_2} \right) \Delta\tau \quad , \qquad (5.4)$$

where g(t) was the output and f(nΔτ) approximated the input probe characteristics. From equation 5.4, the derivative characteristics were found and then investigated for possible methods of analyzing ion composition.

5.3 Results

An ion density profile was obtained for altitudes from 280 to 940 km. A peak density of 6.1×10^4 ions/cm^3 was measured when the probe was exposed to the ionosphere at a height of 280 km, which was 35 km above the F region peak electron density of 4.45×10^5/cm^3 as determined by simultaneous ionsonde. The measured densities decreased to 1.6×10^4 ions/cm^3 at apogee. The Mother-Daughter profile yielded an ion scale height of 274 km at an altitude of 600 km which indicated an ion temperature of 1730° K.

After applying two correction procedures, it was found that the ion profile corresponded reasonably well with densities measured by the Mother-Daughter technique except for the data obtained below approximately 450 km. The correction terms took into account an inaccurate theoretical value for the transmission coefficient and ion currents which were probably collected because of the large negative

potential of the vehicle.

The ion temperatures, as determined from the slope of the probe characteristics, exhibited large random variations of as much as 1000° K from one ion current curve to the next. The average calculated ion temperature was about 3300° K.

Vehicle potential remained fairly constant during the flight and all the data points were within a range of from -2.1 to -2.5 volts. Because vehicle velocity was not much greater than the most probable ion velocity, vehicle potential was overestimated by .4 volts (due to approximations in the theory). Therefore, the average calculated vehicle potential was -1.9 volts.

Current oscillations at the same frequency as the spin rate of the rocket were observed throughout the flight. These current variations distorted the shape of the probe characteristics and consequently, no ion composition calculation could be made.

An electron current was not collected during the electron mode of operation and therefore, electron temperature could not be calculated.

Theoretically, no significantly improved methods of determining ion composition were found from the investigation of the derivative of the probe characteristics, and the derivative characteristics varied only slightly as a function of the differentiator time constant.

5.4 Conclusions

The measured ion densities were not in good agreement with the results of the Mother-Daughter experiment or ionosonde data and there were three significant factors causing the resultant

ion density profile of Figure 17.

Below 450 km, the wake of the Daughter caused a trail of depleted ion densities and resulted in the measured ion densities being extremely low. This wake extended to a distance of the order of 100 m.

On the basis of the fairly constant difference between the ion and electron profiles of Figure 17 for altitudes between 450 and 700 km, it is concluded that the measured ion densities are low by approximately 50% and that the majority of this error is due to an inaccurate geometrical determination of the grid transmission coefficient. Examples from literature in the field verified that geometrical values of α_1 can be 15% higher than true values and this would result in the calculated ion densities being low by approximately the amount they are inaccurate in Figure 17.

The combined electrical transparency of four charged parallel grids to positive ions is not equal to the optical transparency. The total transmission factor cannot be determined by simply raising the optical transparency to a power equal to the number of grids, and the electrical transparency of negatively-charged grids to positive ions is less than the optical transparency.

Above 700 km, vehicle velocity was no longer much greater than the most probable ion velocity and the angle of attack was becoming larger. This combined with the attracting electric field and the ion sheath so that the ion currents were too large and yielded high densities.

Both the ion trajectory analysis and the $f(\phi)$ function indicated that an excess current (not accounted for by the theory)

was collected at the higher altitudes because of the attracting field. Considering this source of error, the calculated densities would approximate the correct values. Thus, it was concluded that it was the large negative potential of -1.9 volts which caused considerable error in the ion density profile above approximately 700 km.

The equations (5.1 - 5.3, and 4.1) used in this analysis are valid for a planar collector mounted on an infinite plane. The influence of the electric field was significant at the higher altitudes where the sheath thickness was becoming large, because this condition was not even approximately satisfied. For attracting potentials, the size and shape of the probe becomes important and an estimate of the influence of the plasma sheath is required to determine the current in an attractive field. The problem is extremely complex since it involves a simultaneous solution of Poisson's equation and a calculation of the ion trajectories. The problem is further complicated by the thermal velocity distribution of the ions.

Ion probes should be mounted flush to conducting plane surfaces of large extent compared to the instrument. As a practical guide, the probe dimensions should be much larger than the sheath thickness. This will help to eliminate any focusing of ions on the probe due to the electric field. This is important if the equations derived by Whipple for planar probes are to yield accurate results.

It was found that the magnitude of the current collected during descent while the probe was in the wake cannot be accounted for by the random thermal velocities of the ions. Near apogee, the density profile was obviously in error. These two effects cannot be interpreted in terms of present probe theory and are related

to the potential of the vehicle, the ion sheath, and the finite dimensions of the probe.

The average ion temperature of 3300° K, as determined from the probe characteristics, was much higher than the value of 1730° K obtained from ion scale height calculations. High ion temperatures have been typical of ion probe experiments (Hanson and McKibbin, 1961, and Hanson et al., 1964) and indicate that theoretical work needs to be done before reasonably accurate temperatures can be obtained with planar traps.

Because of contact potentials, it is difficult to estimate the accuracy of the calculated vehicle potential of -1.9 volts. A contact potential of at least .5 volts between aperture grid and probe surface is reasonable in view of the known work functions of tungsten and aluminum. Then, the vehicle potential is estimated to be -1.4 ± .5 volts. It must be concluded that vehicle potentials are not known nearly as accurately as experimenters would like to believe.

If the contact potential difference between the outer grid and the housing was more than a few tenths of a volt, it would cause ions to be focused on the aperture. This is because the electric field lines (due to potential of the outer grid being more negative than the surrounding aluminum housing) would tend to focus on the aperture grid.

The electric field, due to a contact potential difference, can cause ions to be focused on the aperture and this mechanism has not been considered in earlier experimental work. The fact that this mechanism was neglected is a possible reason why

researchers have not been able to verify theoretically the importance of electric field focusing on ion collection. This mechanism should be considered in analyzing ion currents collected in wakes and the high ion densities which are usually obtained near apogee for instruments flown on vertical sounding rockets.

The difficulties associated with contact potentials could be eliminated by using the same metal throughout the probe assembly. The outer housing, grids, and collector plate should be made from the same metal.

5.5 Suggestions for Future Research

It is recommended that the grid transmission coefficient be determined experimentally in an ion chamber rather than calculated from the geometry of the grid assembly.

The current variations observed throughout the telemetry data were very undesirable and every effort should be made to eliminate them. The probe mounting should be as far removed as possible from any protruding objects. Since the area available for mounting equipment on the payload is rather limited, this may not be so easily accomplished.

Consistent with results presented by Samir and Willmore, relatively large currents were observed while the probe was in the wake of the payload. Near apogee, the calculated densities were high and the profile turned back on itself; a similar profile was described by Anderson et al. (1965). These aspects of the data cannot be reconciled with present theory and there is need of additional theoretical work. A thorough theoretical analysis, giving careful consideration to the interaction of charged particles with the ion

sheath shielding a charged vehicle, is badly needed. Such an analysis should demonstrate how local particle densities and velocity distributions are disturbed by the presence of the probe. It is clear that vehicle potential and velocity, and ion temperature would be important parameters of the analysis.

BIBLIOGRAPHY

Al'Pert, Ja. L., A. V. Gurevic, and L. P. Pitaevskij, Effects Due to an Artificial Earth Satellite in Rapid Motion Through the Ionosphere or the Interplanetary Medium, Space Science Reviews, 2(5), 680-748, 1963.

Anderson, D. N., W. H. Bennett, and L. C. Hale, Temperature and Density in the Ionized Upper Atmosphere at 4000 to 5300 Kilometers, J. Geophys. Res., 70(5), 1031-1038, 1965.

Bauer, S. J. and L. J. Blumle, Mean Diurnal Variation of the Topside Ionosphere at Mid-Latitudes, J. Geophys. Res., 69(17), 3613-3618, 1964.

Bourdeau, R. E., J. L. Donley, G. P. Serbu, and E. C. Whipple, Jr., Measurements of Sheath Currents and Equilibrium Potential on the Explorer VIII Satellite, J. of the Astronautical Sciences, 8(3), 65-73, 1961.

Bourdeau, R. E., J. L. Donley, E. C. Whipple, and S. J. Bauer, Experimental Evidence for the Presence of Helium Ions Based on the Explorer VIII Satellite Data, J. Geophys. Res., 67(2), 467-475, 1962.

Bourdeau, R. E., Ionospheric Research from Space Vehicles, Space Science Reviews, 1(4), 683-728, 1963.

Hale, L. C., Ionospheric Measurements with a Multigrid Retarding Potential Analyzer, Abstract, J. Geophys. Res., 66(5), 1554, 1961.

Hale, L. C., A Probe Assembly for the Direct Measurement of Ionospheric Parameters, Ionosphere Research Laboratory, Pennsylvania State University, Sci. Report No. 223(E), 1964.

Hanson, W. B., and D. D. McKibben, An Ion Trap Measurement of the Ion Concentration Above the F_2 Peak, J. Geophys. Res., 66(6), 1667-1671, 1961.

Hanson, W. B., Upper Atmosphere Helium Ions, J. Geophys. Res., 67(1), 183-188, 1962.

Hanson, W. B., D. D. McKibbin, and G. W. Sharp, Some Ionospheric Measurements with Satellite-Borne Ion Traps, J. Geophys. Res., 69(13), 2747-2763, 1964.

Istomin, V. G., Suprathermal O^+ Ions in the Upper Atmosphere, Cosmic Research, 1(2), 217-221, 1963.

Jastrow, R., and C. A. Pearse, Atmospheric Drag on the Satellite, J. Geophys. Res., 62(3), 413-423, 1957.

Krassovsky, V. I., Exploration of the Upper Atmosphere with the Help of the Third Soviet Sputnik, Proc. of I.R.E., 47(2), 289-296, 1963.

Nagy, A., L. H. Brace, G. Carignan, and M. Kanal, Direct Measurements Bearing on the Extent of Thermal Non-equilibrium in the Ionosphere, J. Geophys. Res., 68(24), 6401-6412, 1963.

Pokhunkov, A. A., Mass-Spectrometric Measurements of the Distribution of He^+, N^+, O^+, NO^+ and O_2^+ Ions in the Earth's Atmosphere Up to a Height of 430 km, Cosmic Research, 1(2), 222-224, 1963.

Sagalyn, R. C., M. Smiddy, and J. Wisnia, Measurement and Interpretation of Ion Density Distributions in the Daytime F Region, J. Geophys. Res., 68(1), 199-211, 1963.

Sagalyn, R. C., and M. Smiddy, Electrical Processes in the Night-time Exosphere, J. Geophys. Res., 69(9), 1809-1823, 1964.

Samir, U., and A. P. Willmore, The Distribution of Charged Particles Near a Moving Spacecraft, Planetary and Space Science, 13(4), 285-296, 1965.

Schwartz, M., Information Transmission, Modulation, and Noise, McGraw-Hill, New York, 1959.

Taylor, H. A., Jr., L. H. Brace, H. C. Brinton, and C. R. Smith, Direct Measurement of Helium and Hydrogen Ion Concentrations and Total Ion Density to an Altitude of 940 Kilometers, J. Geophys. Res., 68(19), 5339-5347, 1963.

Whipple, E. C., Jr., The Ion Trap Results in "Exploration of the Upper Atmosphere with the Help of the Third Soviet Sputnik", Proc. of I.R.E., 47(11), 2023-2024, 1959.

Whipple, E. C., Jr., The Equilibrium Electric Potential of a Body in the Upper Atmosphere and in Interplanetary Space, Ph. D. Thesis, The George Washington Univ., June, 1965.

APPENDIX A

A Computer Program to Solve for the Differentiator Output

A computer program was written to solve equation 2.19 so that the output of the differentiator could be obtained. The computations were done on the IBM 7074 digital computer at the Computation Center of the Pennsylvania State University. The constants in the program were determined from the considerations discussed in section 2.3, and some of the constants had to be adjusted, depending upon the values of τ_1 and τ_2 for a particular program run. The following program was used to solve equation 2.19 for $\tau_1 = .02$ sec and $\tau_2 = .0015$ sec:

```
      COMPILE RUN FORTRAN
      READ 1, D, V, W1, W2, TEMP, T1, T2, T4, NUM
    1 FORMAT(8F10.2/I4)
      DIMENSION AMP(1001)
      AREA=5.07E-4
      Q=1.602E-19
      PI=3.1416
      P=V*SQRTF(PI)
      E=2.718
      C=Q*AREA*V*.25
      CG=1./(1./T2-1./T1)
      C1=-CG/(T1*T2)
      C2=CG/T2**2
      R1=1./SQRTF(W1)
      R2=1./SQRTF(W2)
      Y1=SQRTF(2.*Q)*R1
      Y2=SQRTF(2.*Q)*R2
      B=1.38E-23
      A=SQRTF(2.*B*TEMP)
      A1=A*R1
      A2=A*R2
      DO 100 K=1,5
      Z=K-1
      D1=(1.-Z/4.)*D
      D2=D-D1
      DO 3 I=2,1001
      Y=I-1
      M=I+3999
      TIME=Y*T4
      VOLT=16.41*TIME
```

```
 10 R=SQRTF(VOLT)
 13 X1=(V-Y1*R)/A1
    X2=(V-Y2*R)/A2
    AMP1=C*D1*(A1/(P*E**(X1**2))+1.+2.*ERF(X1*1.4142))
    AMP2=C*D2*(A2/(P*E**(X2**2))+1.+2.*ERF(X2*1.4142))
  3 AMP(M)=AMP1+AMP2
    DO100J=1,16
    W=J-1
    T=W*.01
    VOLTS=16.41*T
    L3=T/T4+4000.
    L2=L3-NUM
 44 SUM=.0
 45 DO 90I=L2,L3
    F=I-4000
    BIG=(T-F*T4)/T2
    IF(BIG-7.) 58,53,53
 53 IF(F) 54,54,55
 54 G=(11.78E-9)*C1/E**((T-F*T4)/T1)*T4
    GO TO 90
 55 G=AMP(I)*C1/E**((T-F*T4)/T1)*T4
 58 IF(F) 59,59,60
 59 G=(11.78E-9)*(C1/E**((T-F*T4)/T1)+C2/E**((T-F*T4)/T2))
       *T4
    GO TO 90
 60 G=AMP(I)*(C1/E**((T-F*T4)/T1)+C2/E**((T-F*T4)/T2))*T4
 90 SUM=SUM+G
    PRINT 111, SUM,T,VOLTS
100 CONTINUE
111 FORMAT(1H0,10X,E20.4,10X,F10.4,5X,F10.4)
120 STOP
    END
```

Any symbols not defined withint the following list are defined within the program:

D = ion density

V = rocket velocity

W1 = mass of O^+ ions

W2 = mass of He^+ ions

T1 = τ_1

T2 = τ_2

T4 = $\Delta\tau$

TEMP = ion temperature

ERF(x) = a subroutine which computes $\frac{1}{\sqrt{2\pi}} \int_0^x e^{-x^2/2} dx$

(note that this error function is different from the one defined in equation 2.6)

B = Boltzman's constant

Q = ionic charge

E = base of the natural logarithms

NUM = a number dependent upon the values of τ_1 and τ_2

AREA = collector area

APPENDIX B

Optical Measurements of Grid Transmission Coefficients

It was crucial that the assumption of a lower value of α be supported by laboratory measurements if the data was to be interpreted correctly. However, the necessary ion chamber equipment was not available and the next best method seemed to be optical measurements.

A collimated light source and a photosensitive detector were used to make the measurements. Ambient light was eliminated and the grids were identical to those used on the flight instrument. The following results were obtained, where θ is the angle between the light beam and the perpendicular to the plane of the grids, and the subscripts on α refer to the number of grids:

$\theta = 0^{\circ}$	$\theta = 30^{\circ}$	$\theta = 45^{\circ}$
$\alpha_1 = .85$	$\alpha_1 = .84$	$\alpha_1 = .84$
$\alpha_4 = .48$	$\alpha_4 = .45$	$\alpha_4 = .40$

By measuring the fraction of the area obstructed by the wires, the following theoretical values were obtained:

grid no. 1	$\alpha_1 = .929$
grid no. 2	$\alpha_1 = .935$
grid no. 3	$\alpha_1 = .935$
grid no. 4	$\alpha_1 = .936$
combination of 4 grids (product of the 4 α_1)	$\alpha_4 = .76$

The two sets of data verify that measured values of α are

lower than theoretical values (from geometrical considerations). The difference becomes quite large for a combination of four grids and approaches the value needed to normalize the ion density profile to the Alouette or Mother-Daughter profile.

It is not known how well the light rays approximate ions passing through charged grids and this should be kept in mind before reaching any conclusions. But, the results are favorable and in agreement with the lower value of α needed to correct the ion density profile.